FEDERAL UNIVERSITY OF SANTA CATARINA
TECHNOLOGY CENTER
AUTOMATION AND SYSTEMS DEPARTMENT
UNDERGRADUATE COURSE IN CONTROL AND AUTOMATION ENGINEERING

Isabella Prando Manzini

Direct yaw moment $\mathcal{H}_\infty$ control system to improve vehicle handling stability

Guyancourt, Île-de-France, France
2024

Isabella Prando Manzini

Direct yaw moment $\mathcal{H}_\infty$ control system to improve vehicle handling stability

Final report of the subject DAS5511 (Course Final Project) as a Concluding Dissertation of the Undergraduate Course in Control and Automation Engineering of the Federal University of Santa Catarina.
Supervisor Maud Peyret
Tutor Marcelo Menezes Morato

Guyancourt, Île-de-France, France
2024

Ficha catalográfica gerada por meio de sistema automatizado gerenciado pela BU/UFSC.
Dados inseridos pelo próprio autor.

Manzini, Isabella Prando
Direct yaw moment H-infinity control system to improve vehicle handling stability / Isabella Prando Manzini ; orientador, Marcelo Menezes Morato, coorientadora, Maud Peyret, 2024.
75 p.

Trabalho de Conclusão de Curso (graduação) - Universidade Federal de Santa Catarina, Centro Tecnológico, Graduação em Engenharia de Controle e Automação, Florianópolis, 2024.

Inclui referências.

1. Engenharia de Controle e Automação. 2. Controle Robusto. 3. Dinâmica lateral do veículo. 4. Controle H infinito. 5. Controle direto do momento de guinada. I. Morato, Marcelo Menezes. II. Peyret, Maud. III. Universidade Federal de Santa Catarina. Graduação em Engenharia de Controle e Automação. IV. Título.

Isabella Prando Manzini

Direct yaw moment $\mathcal{H}_\infty$ control system to improve vehicle handling stability

This dissertation was evaluated in the context of the subject DAS5511 (Course Final Project) and approved in its final form by the Undergraduate Course in Control and Automation Engineering

Guyancourt, July 18, 2024.

Dr. Marcelo De Lellis Costa de Oliveira Dr.
Course Coordinator

Examining Board:

Prof. Marcelo Menezes Morato Dr.
Advisor
UFSC/CTC/DAS

Documento assinado digitalmente
Marcelo Menezes Morato
Data: 18/07/2024 16:21:55-0300
CPF: ***.098.789-**
Verifique as assinaturas em https://v.ufsc.br

Maud Peyret Dr.
Supervisor
Ampere Software Technology, Renault Group

Prof. Daniel Ferreira Coutinho, Dr.
Evaluator
UFSC/CTC/DAS

Prof. Eduardo Camponogara, Dr.
Board President
UFSC/CTC/DAS

ACKNOWLEDGEMENTS

First and foremost, I would like to express my deepest gratitude to my family, especially my mother, Mônica Prando Manzini. Her strength, unwavering support, and encouragement have been a constant source of inspiration throughout my academic journey.

I extend my heartfelt thanks to my professors at UFSC (Universidade Federal de Santa Catarina) and ENSE3 (École nationale supérieure de l'énergie, l'eau et l'environnement). Their guidance and inspiration have been invaluable during my studies in Brazil and France.

Special thanks to Professor Marcelo Menezes Morato, my academic advisor, for his insightful feedback and support at various stages of this work.

I am also grateful to Ampere Software Technology for providing me with the opportunity to intern at the Technocenter in Guyancourt. The six months I spent there were incredibly enriching. I am particularly thankful to Maud Peyret, my local supervisor, for her guidance, expertise, and mentorship throughout this project.

To all my friends who supported me during my two years in France, thank you for making this experience truly memorable. I am especially grateful to Beatriz Bicudo, Jonas Michael, Isabele Mangini, Erick Xisto, Genilson Souza, and Nancy Kyamulesere. Your companionship and support have been invaluable as we navigated the challenges of living in a new country. All the hikes and happy memories will always hold a special place in my heart.

DISCLAIMER

Guyancourt, July 18, 2024.

As representative of the Ampere Software Technology in which the present work was carried out, I declare this document to be exempt from any confidential or sensitive content regarding intellectual property, that may keep it from being published by the Federal University of Santa Catarina (UFSC) to the general public, including its online availability in the Institutional Repository of the University Library (BU). Furthermore, I attest knowledge of the obligation by the author, as a student of UFSC, to deposit this document in the said Institutional Repository, for being it a Final Program Dissertation (*'Trabalho de Conclusão de Curso'*), in accordance with the *Resolução Normativa n° 126/2019/CUn*.

Maud Peyret
Ampere Software Technology

ABSTRACT

In the domain of vehicle dynamic control, managing the lateral motion is a crucial topic in order to ensure safety remarks, appropriate handling, as well as the overall driving experience of the car. In particular, control systems that address yaw motion, which focus on maintaining vehicle stability, are a prominent approach in this field. This dissertation introduces a new yaw rate control scheme applying a direct yaw moment $\mathcal{H}_\infty$ method, aimed at enhancing the robustness of the PID controller implemented in real vehicle at Renault. To achieve this goal, initial studies were conducted to explore the implementation of the $\mathcal{H}_\infty$ control scheme using a (linear) bicycle model. Next, two consecutive $\mathcal{H}_\infty$ controllers were developed using consistent weights for real performance objectives. Several validation results using a complex full vehicle model, along with real experimental vehicle tests under critical driving conditions, confirmed the effectiveness of the proposed control system and its overall improvements in vehicle handling and stability. However, the proposed control system demonstrated a sub-optimal trade-off between control input power and reference tracking when compared to the available PID.

Keywords: Lateral stability. Vehicle Motion Control. H-infinity Control. Vehicle Modelling.

RESUMO

No contexto do controle dinâmico de veículos, gerenciar o movimento lateral é crucial para que se possa garantir a segurança, a dirigibilidade adequada e a experiência geral de condução do carro. Em particular, os sistemas de controle que abordam o movimento de guinada, focando na manutenção da estabilidade do veículo, representam uma abordagem proeminente na literatura. A presente monografia apresenta um novo esquema de controle da taxa de guinada usando o método H_∞, destinado a aumentar a robustez do controlador PID implementado em um veículo real na Renault. Para alcançar esse objetivo, estudos iniciais foram conduzidos para explorar a implementação do esquema de controle H_∞ usando um modelo (linear) de ordem reduzida (do tipo “bicicleta"). Em seguida, dois controladores H_∞ foram desenvolvidos usando ponderações consistentes levando em consideração objetivos de desempenho real. Uma série de resultados de validação usando um modelo completo de veículo, juntamente com testes experimentais reais em veículos sob condições críticas de condução, confirmam a eficácia do sistema de controle proposto e suas melhorias gerais na dirigibilidade e estabilidade do veículo. No entanto, o sistema de controle proposto demonstrou uma troca subótima entre a força de entrada de controle e o rastreamento de referência em comparação com o PID disponível.

Palavras-chave: Controle de Movimento de Veículos. Estabilidade Lateral. Controle H-infinito. Modelagem de Veículos.

LIST OF FIGURES

LIST OF TABLES

LIST OF ABBREVIATIONS AND ACRONYMS

4WD	Four-Wheel Drive
4WS	Four-Wheel Steering
ABS	Anti-lock braking system
AREs	Algebraic Riccati Equations
CoG	Center of Gravity
DOF	Degree-of-Freedom
GS	Gain scheduling
LMIs	Linear Matrix Inequalities
LPV	Linear Parameter-Varying
LTI	Linear Time-Invariant
MIMO	Multiple-Input Multiple-Output
PID	Proportional-Integral-Derivative
RMS	Root Mean Square
SISO	Single-Input Single-Output
VMC	Vehicle Motion Control

LIST OF SYMBOLS

$\mathcal{H}_\infty$	H-Infinity
δ	steering wheel angle
V_x	longitudinal velocity
μ	tire/road contact friction coefficient
M_z	yaw moment
$F_{x,ij}$	longitudinal tire force applied to the ij wheel
i	front or rear
j	left or right
F_{yr}	lateral force applied to the rear wheel
M_{brake}	braking moment
δ_{rear}	rear wheel angle
y	lateral position
ψ	yaw angle
V_y	lateral velocity
a_y	lateral acceleration
a_x	longitudinal acceleration
δ_f	front wheel angle
β	sideslip
l_f	distance COG and front axle
l_r	distance COG and rear axle
d	distance between two wheels
m	vehicle mass
I_z	moment of inertia
C_f	cornering stiffness of front tires
C_r	cornering stiffness of rear tires
λ_{ij}	wheels ij longitudinal slip ratio tire slip ratio
$F_{y,ij}$	lateral tire force applied to the ij wheel
α_{ij}	wheels ij sideslip angle
V	vehicle forward speed
I_w	wheel inertia
$\dot{\omega}$	wheel angular acceleration
R_ω	wheel radius
T_e	driving torque
T_b	braking torque
F_{yf}	lateral force applied to the front wheel
α_f	tire slip angle applied to the front wheel
α_f	tire slip angle applied to the rear wheel

V_{yf}	lateral velocity projected at the front wheel
V_{yr}	lateral velocity projected at the rear wheel
$r(t)$	reference
$u(t)$	control input
$d_i(t)$	input disturbance
$S(s)$	sensitivity function
$T(s)$	complementary sensitivity function
$S(s)G(s)$	plant sensitivity function
$K(s)S(s)$	controller sensitivity function
$L(s)$	open-loop transfer function
$K(s)$	controller
$G(s)$	plant transfer function
$P(s)$	generalized plant
$w(t)$	external input
$z(t)$	controlled output
$T_{zw}(s)$	closed-loop transfer function
$W_e(s)$	non-singular weighting matrix on the error
$W_u(s)$	non-singular weighting matrix on the control
$W_d(s)$	non-singular weighting matrix on the disturbance

CONTENTS

1 INTRODUCTION

[Modified version due to confidentially] In the domain of dynamic motion control for road vehicles, managing the lateral movement is a crucial topic in order to ensure safety, appropriate handling and the overall driving experience of the car. In particular, control systems that address yaw motion aspects, which focus on maintaining vehicle stability, are a prominent approach in this field, such as the yaw stability control system (ARIPIN, M. et al., 2014).

Good handling performance is especially important in high-speed driving and emergency maneuvers. Additionally, road vehicles often encounter challenging conditions, such as wet or icy surfaces. Managing lateral dynamics helps maintain stability under these conditions, preventing the vehicle from sliding or losing grip.

1.1 MOTIVATION AND CONTEXT

Across the various perspectives and developments of the Chassis team at Ampere Software Technology, the objectives considered are the control of various actuators linked to the vehicle's chassis, aiming to enhance both passenger comfort and dynamic behavior. These actuators are practically implemented through a variety of systems, including differential braking, dampers, lateral stability control and even management of the Four-Wheel Steering (4WS) system. Furthermore, it is possible to adjust the vehicle's behavior according to driver preferences, offering driving modes such as "sport", "normal" or "comfortable".

Within the research team where the student was assigned, there is a significant project called Vehicle Motion Control (VMC). The project's main objective is to maintain vehicle stability and handling performance, especially during sudden maneuvers or challenging road conditions. These objectives ensure that the vehicle can adhere to the intended path without experiencing understeer or oversteer, as displayed in Figure 1.

Figure 1 – Cornering vehicle.

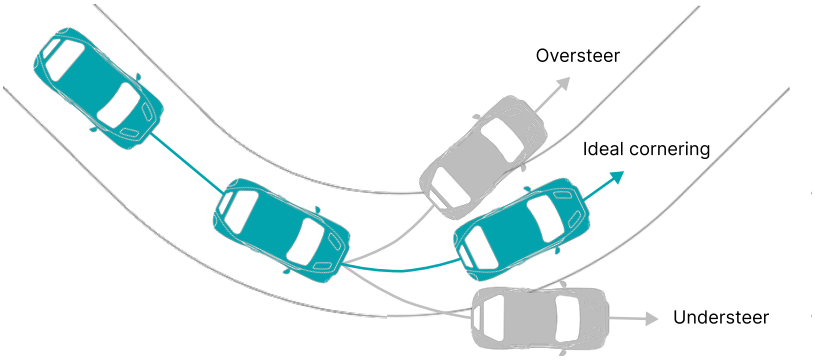

Source: The Author.

When the vehicle's control system detects a potential instability, it can intervene by applying selective braking to individual wheels or adjusting the rear steering angle to help correct the vehicle's trajectory. By selectively applying braking force to specific wheels, the system can effectively counteract oversteer or understeer tendencies, helping the vehicle maintain its intended path. More details of the project will be presented in the next Section.

1.2 VEHICLE MOTION CONTROL PROJECT

In the context of a vehicle, a system of coordinates can be defined by three axes: the vehicle forward motion is depicted along the positive x-axis, the lateral motion is depicted along the y-axis, being positive when oriented towards the driver's left side and the z-axis represents the vertical motion. The rotations around the x, y and z axes are known as roll, pitch and yaw, respectively, as displayed in Figure 2.

Figure 2 – System of coordinates of a vehicle fixed to CoG.

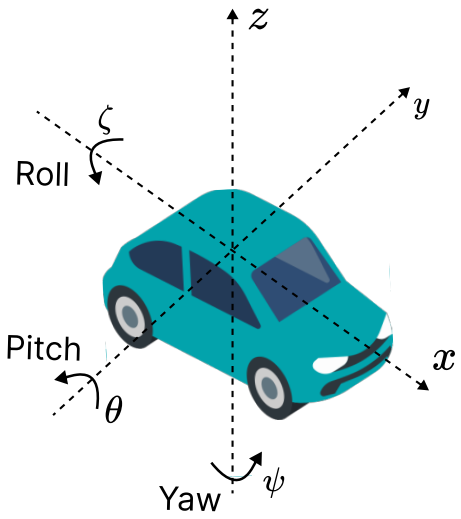

Source: The Author.

The research problem investigated within the context of this work is how to control the lateral motion of the vehicle, which can be measured by the yaw rate and the side slip angle. In particular, by regulating these variables can be achieved by applying a rotational force around the vertical axis or by steering the front wheels of the car, which will consequently rotate the *z* axis. The choice between these methods depends mainly on the actuators available in the vehicle.

As part of the VMC, the company proposed coordinating and optimizing differential braking, which uses the Anti-lock braking system (ABS) brake system on the vehicle to apply differential braking between the right and left wheel to control yaw moment and steer-by-wire, which modify the driver's steering angle input and add a correction steering angle to the rear wheel. The project operates in a closed-loop system, so the vehicle follows a yaw rate reference and optimizes its behavior both at high speed (stability) and low speed (handling). This project is based on a doctoral thesis, (KISSAI, 2019), conducted within the company. A general schematic of the project is presented in Figure 3.

Figure 3 – Scheme of the VMC project.

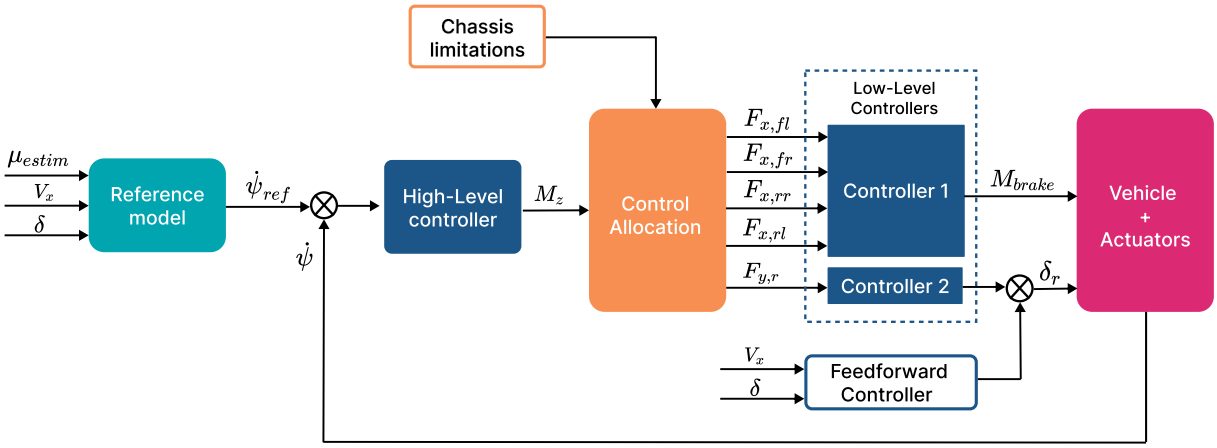

Source: Adapted from Ampere Software Technology (2024).

Next, the role of each one of the seven elements presented in Figure 3 is detailed.

The reference model is used to imposed the overall behavior of the car, which takes into account the driver's commands, including steering angle δ, vehicle longitudinal speed V_x and an estimation of the friction coefficient μ derived from another project under development by the team.

Based on this information, a yaw rate reference $\dot{\psi}_{ref}$ is generated, which serves as input to the High-Level Controller, currently implemented with a Proportional-Integral-Derivative (PID) controller with anti-wind up technique. The controller's parameters are tuned using a lookup table derived from extensive tests that consider longitudinal velocity and lateral acceleration.

This controller generates a yaw moment M_z, which is then sent to the Control Allocation, taking into account Chassis Limitations and optimization methods to achieve the best outcome distribution between the four wheels. The control allocation can also be weighted based on different adhesion to improve comfort and stability in the vehicle, for example in a wet road, the best option is to prioritize braking than the steering wheel angle, so changing this weight is possible to find the best trade-off between performance and comfort.

This results in five outputs: the first four forces $F_{x,ij}$ represent the traction distribution at each wheel, with i = {front,rear} and j = {left,right}, corresponding to a Four-Wheel Drive (4WD) vehicle, while the last one F_{yr} represents the force generated by the steering angle. Finally, the low-level control generates a braking moment M_{brake} and a rear steering angle δ_{rear}, that it is added to the output of the Feedforward Controller, implemented using a bicycle model. Finally, the M_{brake} and δ_{rear} are then send to the vehicle actuators.

For one of the milestone of the project, which aims to mark progress and identify significant achievements in the project lifecycle, it was proposed to evaluate whether the

current PID controller is the most robust option available. To achieve this, a comparison with a robust control method, capable of handling uncertainties and non-linearities, was suggested. In this context, the $\mathcal{H}_\infty$ controller was proposed as a viable alternative. The student's work was therefore developed within this framework. The following Section will detail the objectives of the dissertation.

1.3 OBJECTIVES

The primary objective of this dissertation is to develop a new High-Level controller for the VMC project that offers enhanced robustness compared to the current system. Recent testing has unveiled that the existing High-Level Control system is stable for all cases, however it is seen a reduction in performance when handling variations in vehicle mass. When the vehicle is overloaded, the control can not in all cases regulate the yaw rate to match the reference value. Moreover, as this controller relies on a lookup table for its operation, its effectiveness hinges on the accuracy and granularity of the data used to populate this table. In situations where the table fails to sufficiently cover the entire spectrum of operating conditions, it may result in sub-optimal controller performance. Additionally, the development of such a lookup table demands extensive testing to ensure its accuracy and reliability across diverse driving scenarios. This process requires a significant investment of time and effort from the engineers and technicians responsible.

Given that vehicle's parameters naturally vary, such as wheel radius, tire stiffness, mass, among others and can change over the car's lifespan, along with the unpredictable nature of road conditions including changes in the coefficient of adhesion μ, it is required that the control be robust to these variations. To address this challenge, the use of an $\mathcal{H}_\infty$ control has been proposed, as well as a Gain-Scheduling PID controller with $\mathcal{H}_\infty$ method.

1.4 DOCUMENT OUTLINE

This document presents the development of two $\mathcal{H}_\infty$ controllers. Both controllers demonstrated robustness and good performance in simulation tests, while the controller with the second scheme also performed very well in real vehicle tests. Additionally, a third controller, a PID gain scheduling controller, is introduced and discussed.

The dissertation is divided into five chapters to detail the development of the proposed yaw rate controller.

Chapter 1 explores the context and motivation for the VMC project, within which this dissertation is contained. It details the issues that necessitated the student's work and outlines the objectives of the research scope.

Chapter 2 addresses the theoretical background essential for understanding the subsequent chapters. It outlines key concepts such as stability margins, sensitivity functions, $\mathcal{H}_\infty$ controller and robust PID controller.

Chapter 3 focuses on the presentation of the practical work. It explains the implementation of the $\mathcal{H}_\infty$ controller theory discussed in Chapter 2, summarizing its development and testing. This chapter demonstrates the overall performance of the controller in both simulation and real vehicle scenarios, compares it with the current PID controller and concludes which controller is best suited for use in the VMC project.

Given the conclusion provided from Chapter 3, **Chapter 4** presents a strategy of PID controller with gain scheduling, which adjusts its PID gains based on varying operating conditions or system parameters, offering adaptive control.

Finally, **Chapter 5** concludes the work and discusses the result of the dissertation compared to the initial objectives. It also provides an outlook on further work regarding the VMC project.

2 THEORETICAL BACKGROUND

This chapter provides a theoretical overview of key topics relevant to the dissertation. In the first Section, trajectory control for assisted vehicles is outlined, with a focus on lateral and longitudinal control and their variables of interest. The second and third Sections address nonlinear and linear vehicle models, respectively, summarizing the development of these models. The fourth and fifth Sections delves into stability margins and sensitivity functions, an essential concepts for understanding the content of future chapters. The sixth and seventh Sections explains the theory of $\mathcal{H}_\infty$ synthesis and robust PID controller.

2.1 TRAJECTORY CONTROL FOR AUTONOMOUS AND ASSISTED VEHICLES

Trajectory control plays an essential role in enabling the autonomy and assistance features of modern vehicles. This control mechanism involves guiding the vehicle along a predefined path or trajectory, ensuring precise navigation and safe maneuvering in various driving scenarios. For that there are two main controllers involved, lateral and longitudinal control (RAJAMANI, 2012). Figure 4 demonstrates the vehicle's main variables of interest, considering a cornering manoeuvre.

Figure 4 – Scheme representing the nonlinear dynamics of a vehicle in motion.

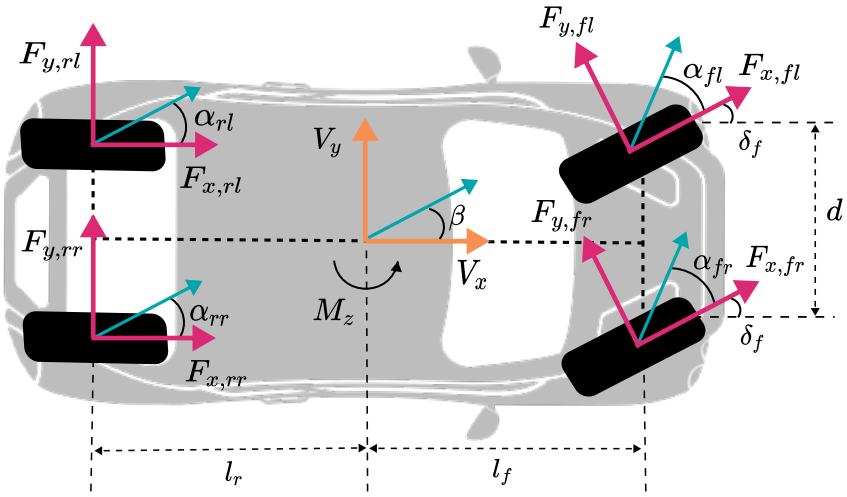

Source: The Author.

2.1.1 Lateral control

The main objective of lateral control is to maintain the vehicle's position and trajectory in the horizontal direction, perpendicular to the direction of path (CHEN, C.; TOMIZUKA, 2000). The variables of interest in lateral control include:

- Lateral Position y: The lateral position of the vehicle within its lane or desired trajectory.
- Yaw Angle ψ: The orientation of the vehicle's longitudinal axis relative to its direction of travel.
- Yaw Rate $\dot{\psi}$: The rate of change of the vehicle's yaw angle over time.
- Steering Angle δ: The angle of the front wheels, which determines the direction of lateral motion.
- Lateral Velocity V_y: The rate of lateral motion of the vehicle.
- Lateral Acceleration a_y: The acceleration experienced by the vehicle in the transverse direction.

2.1.2 Longitudinal control

Contrary to lateral control, the main objective of longitudinal control is to manage the vehicle's acceleration and braking, ensuring smooth and safe movement along the desired path (NAEEM; MAHMOOD, 2017).

- Longitudinal velocity V_x: The velocity of the vehicle in the direction of travel.
- Longitudinal acceleration a_x: The rate of change of velocity over time, which can be positive (acceleration) or negative (braking).

In sum, these two controllers complement each other in terms of motion control of the vehicle. Lateral control manages the vehicle's sideways motion, ensuring it stays within the desired path and yaw rate, while longitudinal control regulates the vehicle's speed and longitudinal position. By working together, these controllers ensure precise maneuvering, stabilityand safety in various driving scenarios, enhancing the overall control and performance of the vehicle.

2.2 NONLINEAR VEHICLE MODEL

The nonlinear vehicle model is regularly used to represent and simulate the actual vehicle for controller evaluation and validation. It can present different numbers of Degree-of-Freedom (DOF), representing the dynamics and complexity of the model. The one detailed in this section has seven DOF, which includes the longitudinal, lateral, yawand four wheels dynamic motion, as detailed in (ZHAO; XIANG; RICHARDSON, 2006).

Such model can be analysed in terms of four variable categories: input, output, vehicle parameters and variables of interest. The inputs consist of the front wheel angle

δ_f and yaw moment $M_Z$and the outputs to be controlled are vehicle sideslip β and yaw rate $\dot{\psi}$. The vehicle parameters are defined by the distance from CoG to the front/rear axle l_f, l_r, the distance between two wheels d, vehicle mass m, moment of inertia I_Z and front/rear tire cornering stiffness C_f, C_r. The variables of interest are then the longitudinal velocity V_x and acceleration a_x, lateral velocity V_y and acceleration a_y.

Longitudinal tire forces $F_{x,ij}$, where i = {front, rear} and j = {left, right}, depend proportionally to the tire slip ratio in each wheel λ_{ij}, while the lateral tire forces $F_{y,ij}$ depend proportionally to the tire sideslip angle in each wheel α_{ij}. For larger slip angles and slip ratios, longitudinal and lateral tire forces exhibit nonlinearities, needing more complex models to detail the tire behaviour, such as the Pacejka tire model as detailed in (PACEJKA, 2006) or the Dugoff tire model as used in (DU; ZHANG; NAGHDY, 2011).

The vehicle dynamic equilibrium equations for longitudinal motion can be expressed as:

$$\begin{aligned} ma_x(t) &= m\left(\dot{V}_x(t) - \dot{\psi}\,V_y(t)\right) \\ &= \left(F_{x,fl}(t) + F_{x,fr}(t)\right) cos\ \delta_f(t) + F_{x,rl}(t) + F_{x,rr}(t) - \left(F_{y,fl}(t) + F_{y,fr}(t)\right) sin\ \delta_f(t). \end{aligned} \tag{1}$$

The lateral motion can be expressed as:

$$\begin{aligned} ma_y(t) &= m\left(\dot{V}_y(t) - \dot{\psi}\,V_x(t)\right) \\ &= \left(F_{x,fl}(t) + F_{x,fr}(t)\right) sin\ \delta_f(t) + F_{x,rl}(t) + F_{x,rr}(t) + \left(F_{y,fl}(t) + F_{y,fr}(t)\right) cos\ \delta_f(t). \end{aligned} \tag{2}$$

The yaw motion can be expressed as:

$$\begin{aligned} I_Z\ddot{\psi}(t) &= l_f\left(F_{y,fl}(t)\ cos\ \delta_f(t) + F_{y,fr}(t)\ cos\ \delta_f(t) + F_{x,rl}(t)\ sin\ \delta_f(t) + F_{x,rr}(t)\ sin\ \delta_f(t)\right) \\ &\quad - l_r\left(F_{y,rl}(t) + F_{y,rr}(t)\right) + M_Z(t). \end{aligned} \tag{3}$$

In Equation (2), the lateral acceleration can be expressed in terms of vehicle forward speed, yaw rate and sideslip angle:

$$\begin{aligned} a_y(t) &= \dot{V}_y(t) + \dot{\psi}\,V_x(t) \\ &= V(t)\ (\dot{\psi}(t) + \dot{\beta}(t)). \end{aligned} \tag{4}$$

Therefore, replacing Equation (4) by Equation (2) and isolating the sideslip angle variable (β), one obtains:

$$\dot{\beta}(t) = \frac{1}{mV(t)}\left[cos\ \beta(t)\left(cos\ \delta_f(t)\left(F_{x,fl}(t) + F_{x,fr}(t)\right) - sin\ \delta_f(t)\left(F_{y,fl}(t) + F_{y,fr}(t)\right)\right)\right. \tag{5}$$

$$\left. -sin\ \beta(t)\left(sin\ \delta_f(t)\left(F_{x,fl}(t) + F_{x,fr}(t)\right) - sin\ \delta_f(t)\left(F_{y,fl}(t) + F_{y,fr}(t)\right)\right)\right] - \dot{\psi}. \tag{6}$$

The derivative of the yaw rate can be obtained from the Equation (3) as follows

$$\ddot{\psi} = \frac{1}{I_z}\Big[I_f\Big(F_{y,fl}(t)\ cos\ \delta_f(t) + F_{y,fr}(t)\ cos\ \delta_f(t) + F_{y,rl}(t)\ sin\ \delta_f(t) + F_{y,rr}(t)\ sin\ \delta_f(t)\Big) \\ -I_r\Big(F_{y,rl}(t) + F_{y,rr}(t)\Big) + M_z(t)\Big]. \tag{7}$$

To complete the last four DOF The dynamic motion of each wheel represents one DOF, defined as

$$I_w\dot{\omega}_{ij}(t) = -R_{\omega\,ij}F_{x\,ij}(t) + T_{e\,ij}(t) - T_{b\,ij}(t), \tag{8}$$

where I_w is the wheel inertia, $\dot{\omega}$ is wheel angular acceleration, R_ω wheel radius, T_e is braking torque and T_b is driving torque.

Using this model, it is possible to approximate the behavior of a real vehicle and use it for testing and validation. However, models with higher DOF, such as eight DOF used in (WU et al., 2010) and (DING; TAHERI, 2010) or fourteen DOF used in (LACROIX; LIU, Z. H.; SEERS, 2012) and (CANALE; FAGIANO, 2010), provide more accurate simulations and validations by capturing additional dynamic complexities.

2.3 LINEAR VEHICLE MODEL

The vehicle model presented in Section 2.2 can be reduced to a linear bicycle model, which simplifies the representation of the vehicle's lateral and yaw motions (ZHOU, Hongliang; LIU, Z., 2010). In order to achieve this reduction, several assumptions and simplifications are necessary to linearize the model. The left and right wheels at the front and rear axle are considered as a single wheel at the centerline of the vehicle. No braking is applied at any wheel and the CoG is not shifted as vehicle mass changes. A global scheme of the model can be seen in Figure 5.

Figure 5 – Vehicle scheme of the (linear) bicycle model.

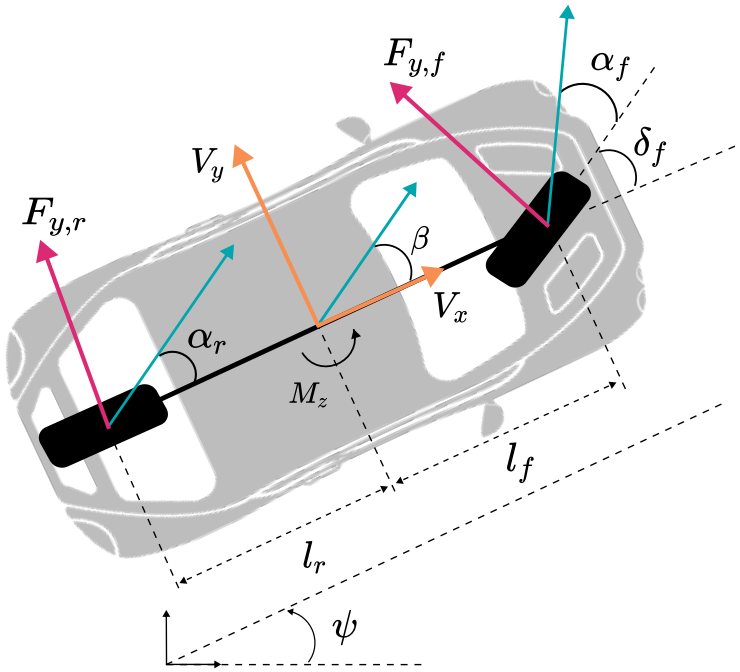

Source: The Author.

The input of the model is the front wheel steer angle δ_f and the yaw moment M_z, while the output variables to be controlled are the vehicle sideslip β and yaw rate $\dot{\psi}$. The parameters of the vehicle include the distance from CoG to the front/rear axle l_f, l_r, the distance between two wheels d, vehicle mass m, moment of inertia I_z and front/rear tire cornering stiffness C_f, C_r. The variables of interest are longitudinal velocity V_x and acceleration a_x, lateral velocity V_y and acceleration a_y.

The vehicle moves on a plane and dry road. This model consists of 2 DOF for lateral and yaw motion. Using the Fundamental Principles of Dynamics for lateral motion:

$$Ma_y(t) = F_{yf}(t) + F_{yr}(t). \tag{9}$$

Assuming that the system remains in the zone of linear tire behavior, the lateral tire forces F_{yf}, F_{yr} depend directly on the tire slip angle in each wheel α_f, α_f. For smaller slip angles and slip ratios, the lateral tire force is described as a linear function of the tire cornering stiffness and tire slip angle as follows:

$$\begin{cases} F_{yf} = C_f \alpha_f(t), \\ F_{yr} = C_r \alpha_f(t). \end{cases} \tag{10}$$

The lateral motion is define as:

$$M(\dot{V}_y(t) + \dot{\psi}(t) V_x(t)) = C_{\alpha f} \alpha_f(t) + C_{\alpha r} \alpha_r(t), \tag{11}$$

with

$$\begin{cases} \alpha_f(t) = \delta_f - \tan^{-1}\left(\frac{V_{yf}(t)}{V_{xf}(t)}\right), \\ \alpha_r(t) = \tan^{-1}\left(\frac{V_{yr}(t)}{V_{xr}(t)}\right), \end{cases} \tag{12}$$

where V_{yf} is the lateral velocity projected onto the front wheel and V_{yr} is longitudinal velocity projected onto the rear wheel. Since there is no rotation of the x and y axis, pitch and roll are neglected, results in:

$$\begin{cases} V_{xi}(t) = V_x(t), \\ V_{yi}(t) = V_y(t) + L_i\dot{\psi}(t), \\ V_{zi}(t) = V_z(t), \end{cases} \tag{13}$$

being i = {front, rear}. Replacing the Equation (13) in Equation (12) arrives to:

$$\alpha_f(t) = \delta_f(t) - \tan^{-1}\left(\frac{V_y(t) + l_f\dot{\psi}(t)}{V_x(t)}\right).$$

Assuming the hypothesis of dealing with small angles, $\tan^{-1}(x) \approx x$:

$$\alpha_f(t) \approx \delta_f(t) - \left(\frac{V_y(t) + l_f\dot{\psi}(t)}{V_x(t)}\right). \tag{14}$$

Using the same process for the rear wheel:

$$\begin{aligned} \alpha_r(t) &= -\tan^{-1}\left(\frac{V_y(t) + l_r\dot{\psi}(t)}{V_x(t)}\right), \\ &\approx -\left(\frac{V_y(t) + l_r\dot{\psi}(t)}{V_x(t)}\right). \end{aligned} \tag{15}$$

Returning to Equation (11) and incorporating the results from Equation (14) and Equation (15) yields to:

$$M(\dot{V}_y(t) + \dot{\psi}(t)\dot{V}_x(t)) = C_{\alpha f}\left(\delta_f(t) - \frac{V_y(t) + l_f\dot{\psi}(t)}{V_x(t)}\right) + C_{\alpha r}\left(-\frac{V_y(t) + l_r\dot{\psi}(t)}{V_x(t)}\right). \tag{16}$$

Since the sideslip angle is defined by:

$$\beta(t) = \frac{V_y(t)}{V_x(t)}.$$

Its derivative is therefore:

$$\dot{\beta}(t) = \frac{\dot{V}_y(t)V_x(t) - V_y(t)\dot{V}_x(t)}{V_x^2(t)} = \frac{\dot{V}_y(t)}{V_x(t)} - \frac{V_y(t)\dot{V}_x(t)}{V_x^2(t)}.$$

Considering that the longitudinal velocity Vx is constant, it can be neglecting the longitudinal acceleration resulting in:

$$\dot{\beta}(t) \approx \frac{\dot{V}_y(t)}{V_x}. \tag{17}$$

Replacing equation Equation (17) in Equation (11) and simplifying it, it is possible to find:

$$\dot{\beta}(t) = \delta_f(t)\left(\frac{C_{\alpha f}}{MV_x}\right) - \beta(t)\left(\frac{C_{\alpha f} + C_{\alpha r}}{MV_x}\right) + \dot{\psi}(t)\left(\frac{-C_{\alpha f}l_f + C_{\alpha r}l_r}{MV_x^2} - 1\right). \tag{18}$$

For the yaw motion, using the Fundamental Principles of Dynamics:

$$I_z\ddot{\psi}(t) = l_f F_{yf}(t) - l_r F_{yr}(t).$$

With the hypotheses made for this model, write:

$$\ddot{\psi}(t) = \delta_f(t)\left(\frac{l_f C_{\alpha f}}{I_z}\right) - \beta(t)\left(\frac{l_f C_{\alpha f} - l_r C_{\alpha r}}{I_z}\right) - \dot{\psi}(t)\left(\frac{{l_f}^2 C_{\alpha f} + {l_r}^2 C_{\alpha r}}{I_z V_x}\right). \tag{19}$$

Finally, the following state representation is found for the vehicle lateral dynamics:

$$\begin{cases} \dot{\beta}(t) = \delta_f(t)\left(\frac{C_f}{MV_x}\right) - \beta(t)\left(\frac{C_f + C_r}{MV_x}\right) + \dot{\psi}(t)\left(\frac{-C_f l_f + C_r l_r}{MV_x^2} - 1\right), \\ \ddot{\psi}(t) = \delta_f(t)\left(\frac{l_f C_f}{I_z}\right) - \beta(t)\left(\frac{l_f C_f - l_r C_{\alpha r}}{I_z}\right) - \dot{\psi}(t)\left(\frac{{l_f}^2 C_{\alpha f} + {l_r}^2 C_r}{I_z V_x}\right). \end{cases} \tag{20}$$

With a matrix state space representation of:

$$\begin{bmatrix} \dot{\beta}(t) \\ \ddot{\psi}(t) \end{bmatrix} = \begin{bmatrix} -\frac{C_f + C_r}{MV_x} & -\frac{C_f l_f - C_r l_r}{MV_x^2} - 1 \\ -\frac{C_f l_f - C_r l_r}{I_z} & -\frac{C_f {l_f}^2 + C_r {l_r}^2}{I_z V_x} \end{bmatrix} \begin{bmatrix} \beta(t) \\ \dot{\psi}(t) \end{bmatrix} + \begin{bmatrix} \frac{C_f}{MV_x} \\ \frac{l_f C_f}{I_z} \end{bmatrix} \delta_f(t), \tag{21}$$

where the state variables are sideslip β and yaw rate $\dot{\psi}$, with the control input being the front wheel angle δ_f.

In some particular situations, such as those described (LACROIX; LIU, Z. H.; SEERS, 2012) and (ZHOU, Hongliang; LIU, Z., 2010), direct yaw moment control is used. In order to incorporate this variable into the state space represented in Equation (21), it is necessary to establish a relationship between the yaw moment and the state variables. As detailed in (MINOIU ENACHE, 2008) and (ARIPIN, M. K. et al., 2014), the following equation is reached:

$$\ddot{\psi}(t) = \frac{M_Z(t)}{I_z}. \tag{22}$$

By exploiting Equation (22), it is possible to expand the state space as:

$$\begin{bmatrix} \dot{\beta}(t) \\ \ddot{\psi}(t) \end{bmatrix} = \begin{bmatrix} -\frac{C_f + C_r}{MV_x} & -\frac{C_f l_f - C_r l_r}{MV_x^2} - 1 \\ -\frac{C_f l_f - C_r l_r}{I_z} & -\frac{C_f {l_f}^2 + C_r {l_r}^2}{I_z V_x} \end{bmatrix} \begin{bmatrix} \beta(t) \\ \dot{\psi}(t) \end{bmatrix} + \begin{bmatrix} \frac{C_f}{MV_x} \\ \frac{l_f C_f}{I_z} \end{bmatrix} \delta_f(t) + \begin{bmatrix} 0 \\ \frac{1}{I_z} \end{bmatrix} M_Z(t). \tag{23}$$

Typically, if one variable is chosen to be the control input, the other is used as a disturbance to the system.

It cares to be highlighted that the aforementioned "bycicle" model is widely used for control synthesis, but it is also employed as a reference model to generate the desired response based on steady-state conditions or an approximated first-order response. Taking into account that the Equation (35) model is used for synthesis, the next section will present some concepts that will be used to analyze the performance of the control strategies proposed in this work.

2.4 STABILITY MARGINS

Stability margins are fundamental concepts in control theory that provide insights into the stability and robustness of a control system. There are three primary stability margins: gain margin, phase margin and delay margin.

1. **Gain margin**

   The gain margin measures the relative distance from the system's open-loop gain crossover frequency to the critical gain value where the closed-loop system becomes marginally stable.

   $$G_M(dB) = -\ [|L(j\omega_\pi)|]_{dB}\,.$$

   In other words, the gain margin indicates how much the system's gain can be increased before it becomes unstable. A positive gain margin implies stability, while a negative gain margin indicates instability.

2. **Phase margin**

   The phase margin measures the relative phase difference between the system's phase response and -180 degrees at the gain crossover frequency.

   $$\Phi_M = 180^\circ\ +\ arg\,[|L(j\omega_c)|]\,, \text{ where } |L(j\omega_c)| = 0dB.$$

   It represents the system's stability robustness with respect to phase lag. A higher phase margin indicates better stability robustness.

3. **Delay margin**

   The delay margin measures the maximum amount of time delay that can be introduced into the system before it becomes unstable. Time delays in a system can be caused by factors such as computational delays, transmission delays, actuator dynamics and filters. A larger delay margin indicates better robustness to time delays.

Stability margins quantitatively assess a control system's stability and robustness under various conditions, helping in the evaluation and comparison of different designs to meet desired stability and performance specifications. They also analyze the system's robustness against uncertainties and disturbances, with larger margins indicating greater robustness. Additionally, stability margins help identify potential stability issues, where small or negative margins may indicate instability.

2.5 SENSITIVITY FUNCTIONS

In addition to stability margins, sensitivity functions are crucial tools in control theory for analyzing the impact of external signals on the system output. A general control scheme illustrating the main sensitivity functions is presented in Figure 6.

Figure 6 – Block diagram with sensitivity functions.

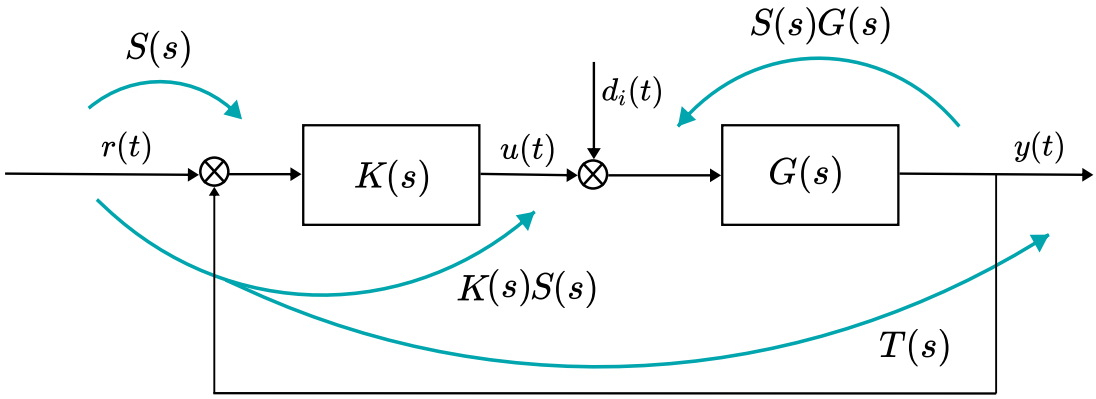

Source: The Author.

In the diagram provided in Figure 6, $r(t)$ represents the reference signal, $u(t)$ the control input, $d_i(t)$ the input disturbance and y(t) the measured output. The four sensitivity functions are $S(s)$ (sensitivity function), $T(s)$ (complementary sensitivity function), $S(s)G(s)$ (plant sensitivity function) and $K(s)S(s)$ (controller sensitivity function). These functions are detailed next.

1. **Sensitivity function (S)**

   The sensitivity function $S(s)$, is defined as:

   $$S(s) = \frac{1}{1 + L(s)}, \tag{24}$$

   where $L(s)$ is the open-loop transfer function of the system defined as:

   $$L(s) = K(s)G(s). \tag{25}$$

   The sensitivity function measures the response of the closed-loop system to changes in the reference input and disturbances. It provides insights into how well the control system can reject disturbances and follow the reference. A lower value of $|S(j\omega)|$ at low frequencies indicates better disturbance rejection and tracking.

2. **Controller Sensitivity function (KS)**

   The controller sensitivity function $K(s)S(s)$, is defined as:

   $$K(s)S(s) = \frac{K(s)}{1 + L(s)}. \tag{26}$$

   where $K(s)$ is the controller transfer function. The controller sensitivity function measures how the control signal responds to changes in the reference input and noise. It provides insights into the effort required by the controller to maintain desired performance and noise attenuation. A lower value of $|KS(j\omega)|$ along all

frequencies indicates that the controller exerts less effort to reject disturbances and track the reference input, which can extent the life of the actuator. Additionally, $|KS(j\omega)| \to \infty$ in high frequencies means there is noise attenuation.

3. **Complementary Sensitivity Function (T)**

   The complementary sensitivity function $T(s)$, is given by:

$$T(s) = \frac{L(s)}{1 + L(s)}. \tag{27}$$

   The complementary sensitivity function measures the response of the system to sensor noise and how changes in the reference affect the response. It is crucial for assessing noise attenuation and reference tracking.

4. **Plant Sensitivity Function (SG)**

   The plant sensitivity function $S(s)G(s)$, is defined as:

$$S(s)G(s) = \frac{G(s)}{1 + L(s)}, \tag{28}$$

   where $G(s)$ is the plant transfer function. The plant sensitivity function measures the effect of disturbances on the plant output. It provides insights into how external inputs affect the closed-loop system's performance. A lower value of $|SG(j\omega)|$ indicates better robustness against input disturbances.

In summary, sensitivity functions are crucial in understanding the performance trade-offs between disturbance rejection and noise sensitivity. They assess the control effort required to maintain desired performance, guiding the design of efficient and balanced control systems. In the context of robust control, specifically the H_∞ controller framework used in this dissertation, sensitivity functions play a pivotal role. They help guide the design of weighting functions used to impose control performance criteria, ensuring the system is stable and can handle uncertainties and disturbances effectively. This will be detailed further in the next section.

2.6 $\mathcal{H}_\infty$ CONTROL

$\mathcal{H}_\infty$ control is a robust control strategy used in control systems to design controllers that can effectively handle uncertainties and disturbances in the system. The goal is to minimize the worst-case gain of the transfer function from the disturbance to the error signal, ensuring that the system remains stable and performs well even in the presence of model uncertainties and external unwanted signals.

A controller can be called robust if ensures system performance and stability under a wide range of operating conditions and model uncertainties. $\mathcal{H}_\infty$ control specifically targets robustness by minimizing the $\mathcal{H}_\infty$ norm. Which in a transfer function is

the maximum singular value of the system's frequency response. It represents the worst-case gain of the system over all frequencies. In the Figure 7 it is possible to see a general scheme of a Single-Input Single-Output (SISO) Linear Time-Invariant (LTI) system with a $\mathcal{H}_\infty$ controller.

Figure 7 – $\mathcal{H}_\infty$ closed-loop transfer function scheme.

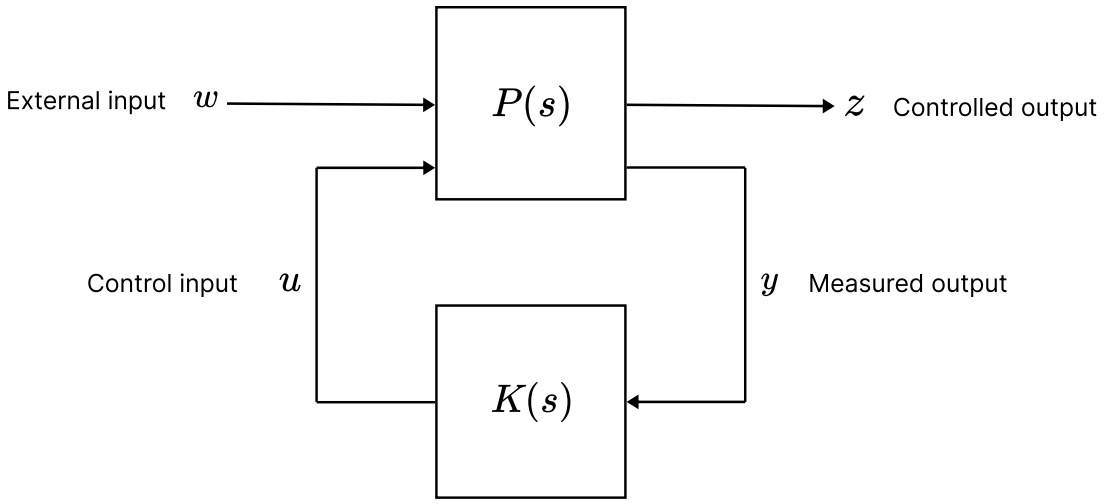

Source: The Author.

In Figure 7, $P(s)$ represents generalized plant (containing the plant and the weights), $K(s)$ the controller, $w(t)$ the external inputs (such as reference, disturbance and noise) and $z(t)$ the plant's controlled outputs.

The main objective of the $\mathcal{H}_\infty$ framework scheme is to design a stabilizing controller $K(s)$ which based on the information in y, generates a control signal u which counteracts the influence of w on z, thereby minimizing the closed-loop norm from w to z less than a specified optimal value γ. Such objective can be formulated as:

$$K(s) = \underset{K(s)}{\operatorname{argmin}} \ \gamma \text{ s.t.} \| T_{zw}(s) \|_\infty \leq \gamma.$$

The closed-loop transfer function includes contributions from the plant $G(s)$, the controller $K(s)$ and weighting functions (templates) that shape the performance and robustness requirements.

Performance templates define the desired performance criteria, such as tracking accuracy, disturbance rejection and noise attenuation. These criteria are translated into weighting functions, which penalize deviations from desired performance. For instance, a template for disturbance rejection might specify high attenuation at low frequencies, resulting in a weighting function that emphasizes these frequencies. Moreover, robustness templates specify the system's tolerance to model uncertainties and external disturbances. These are translated into robustness weighting functions, which penalize control actions that might lead to instability or degraded performance under uncertain-

ties. Some practical examples on how to select appropriate weighting functions are represented next:

1. **Template on the sensitivity function S(s)**

   Typical specifications in terms of $S(s)$ include:

   - Minimum bandwidth frequency ω_s,
   - Maximum tracking error at selected frequencies,
   - Maximum steady-state tracking error ϵ_0,
   - Shape of $S(s)$ over selected frequency ranges,
   - Maximum peak magnitude of $S(s)$ i.e $\|S(s)\|_\infty < M_s$. The peak specification prevents amplification of noise at high frequencies and also introduces a margin of robustness.

   Giving a function in the shape of:

   $$\frac{1}{W_e(s)} = \frac{s + \omega_s \epsilon_0}{\frac{s}{M_s} + \omega_s}. \tag{29}$$

   Mathematically, these specifications may be captured by an upper bound, on the magnitude of $S(s)$:

   $$|S(j\omega)| \leq \frac{1}{|W_e(j\omega)|} \Leftrightarrow \|W_e(s)S(s)\|_\infty \leq 1.$$

2. **Template on the controller sensitivity function K(s)S(s)**

   - Minimum bandwidth frequency ω_u,
   - Noise attenuation ϵ_1.
   - Shape of $K(s)S(s)$ over selected frequency ranges,
   - Maximum peak magnitude of $K(s)S(s)$, $\|K(s)S(s)\|_{-\infty} < M_u$. The peak specification prevents saturation on the actuator.

   Giving a function in the shape of:

   $$\frac{1}{W_u(s)} = \frac{\epsilon_1 + \omega_u}{s + \frac{\omega_u}{M_u}}. \tag{30}$$

   Mathematically, these specifications may be captured by an upper bound, on the magnitude of $K(s)S(s)$:

   $$|K(j\omega)S(j\omega)| \leq \frac{1}{|W_u(j\omega)|} \Leftrightarrow \|W_u(s)K(s)S(s)\|_\infty \leq 1.$$

3. **Template on the complementary sensitivity function T(s)**

   In this dissertation, a direct approach to applying a template to the $T(s)$ will not be explained. Instead, an indirect approach will be presented. Since $T(s)$ is directly influenced by $S(s)$, the sensitivity function will provide an indirect template for $W_u(s)$ and $W_d(s)$, where $W_u(s)$ and $W_d(s)$ represent the templates for the control input and disturbance, respectively. Therefore, the upper bound can be defined as follows:

$$|T(j\omega)| \leq \frac{1}{|W_u(j\omega)W_d(j\omega)|} \Leftrightarrow \|W_u(s)W_d(s)T(s)\|_\infty \leq 1.$$

4. **Template on the plant sensitivity function S(s)G(s)**

   Similarly, for $T(s)$, the sensitivity function $S(s)G(s)$ will also have an indirect template, which can be defined as:

$$|SG(j\omega)| \leq \frac{1}{|W_e(j\omega)W_d(j\omega)|} \Leftrightarrow \|W_e(s)W_d(s)T(s)\|_\infty \leq 1.$$

For a better understanding of how the templates are included in the control scheme, Figure 8 provides an extended representation of Figure 7. It details the components inside the generalized plant, such as the weighting functions W_d, W_e and W_u and the plant $G(s)$.

Figure 8 – Block diagram with mixed weighting functions.

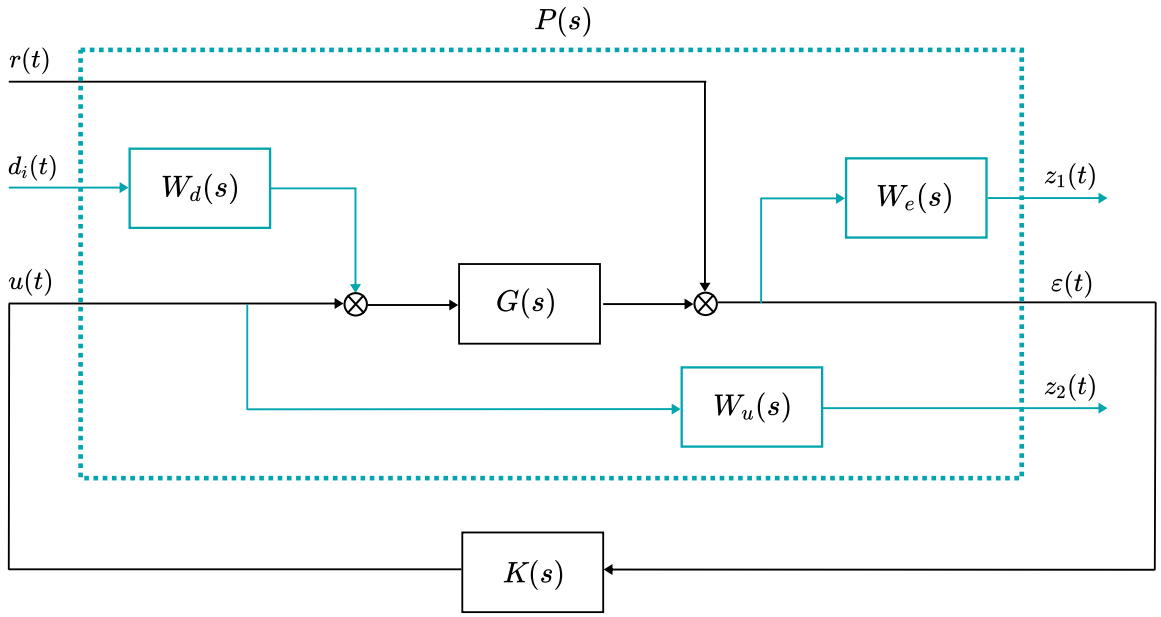

Source: The Author.

The templates are integrated into the $\mathcal{H}_\infty$ optimization problem by defining the generalized plant $P(s)$ that seeks to minimize the $\mathcal{H}_\infty$ norm of the closed-loop transfer function from $w(t)$ to $z(t)$:

$$K(s) = \underset{K(s)}{\operatorname{argmin}} \| T_{zw}(s) \|_\infty \leq \gamma_\infty, \tag{31}$$

subject to:

$$P(s) = \begin{bmatrix} W_e(s) & -W_e(s)G(s) \\ 0 & W_u(s) \\ I & -G(s) \end{bmatrix} \text{ and } \gamma \geq 0 \tag{32}$$

This optimization problem typically involves solving Algebraic Riccati Equations (AREs) (ZHOU, K.; KHARGONEKAR, 1988) or using Linear Matrix Inequalities (LMIs), C.F. (D'ANDREA, 1996).

Besides the strategies presented in this thesis, if the system has a set of parameters that vary in a known way, a Linear Parameter-Varying (LPV) framework can be implemented to ensure robust performance across different operating conditions by dynamically adjusting the controller based on the varying parameters (JIN; YIN; CHEN, N., 2015). Additionally, the $\mathcal{H}_\infty$ control can be extended to σ control, resulting in a robust control strategy defined by a Linear Fractional Transformation (LFT) system (GAO et al., 2016). This extension allows the system to handle unstructured uncertainties more effectively, enhancing the overall robustness and stability of the control system.

Another significant advantage of the $\mathcal{H}_\infty$ controller is its effectiveness in handling Multiple-Input Multiple-Output (MIMO) systems (DOUMIATI, Moustapha et al., 2010). Additionally, $\mathcal{H}_\infty$ controllers can be structured with various configurations such as feedforward, feedback, or a combination of both. This adaptability allows to tailor the control strategy to specific system requirements, optimizing performance and robustness.

2.7 ROBUST PID CONTROL

The $\mathcal{H}_\infty$ controller is a widely recognized robust control method, known for its ability to handle system uncertainties and disturbances. However, its implementation requires an extensive background in control theory. In the industry, most controllers are tuned by technicians who typically lack this specialized knowledge. Consequently, the PID controller is more commonly used.

PID controller boasts several advantages, including its simplicity in implementation and tuning. However, in certain scenarios, it may lack robustness. To address this limitation, a Robust PID Controller can be developed, aiming to enhance stability and performance in systems with uncertainties or dynamic variations. While the conventional PID controller functions effectively under nominal conditions, its robust counterpart offers resilience against parameter fluctuations and disturbances.

Various methodologies exist to implement robust control strategies. Frequency domain analysis tools may be employed to shape the controller's frequency response, ensuring robust performance across diverse operating conditions. In systems exhibiting

non-linearities, the Robust PID Controller may utilize nonlinear compensation techniques to counteract non-linear effects and uphold stability. Some implementations integrate adaptive tuning algorithms, dynamically adjusting controller parameters based on real-time system feedback, thereby augmenting robustness.

Practically, one widely utilized approach, prevalent in industry, involves employing a lookup table (ZHOU, Hao et al., 2015). Rather than relying on a single parameter configuration for all cases, a table is constructed, gathering optimal control inputs for various operating conditions or system states. The controller interpolates between table entries, determining the most suitable control action for the present system state, facilitating smooth and continuous control. While offering enhanced robustness compared to traditional PID controllers, this strategy has drawbacks, notably its inability to guarantee stability beyond the operational range. Additionally, constructing the table requires numerous tests across different operating points.

An alternative approach which ensures parameter-dependent quadratic stability and guaranteed quadratic cost of the closed-loop system, for all uncertain plant parameters is the Gain scheduling (GS) PID Controller (VESELÝ; ILKA, 2013) design. The key idea behind it is to adapt the proportional, integraland derivative gains of the PID controller based on the current operating conditions.

The use of $\mathcal{H}_\infty$ control principles in gain scheduling adds an additional layer of robustness to the PID approach. By leveraging $\mathcal{H}_\infty$ techniques, the gain-scheduled PID controller can maintain stability and performance in the presence of uncertainties and disturbances. This strategy combines the simplicity of PID control with the robustness of $\mathcal{H}_\infty$ principles to achieve optimal performance in diverse and dynamic environments.

In summary, Section 2 and 3 introduced two vehicle models to enhance understanding of vehicle dynamics. Section 4 focused on stability margins, providing a method to assess the stability and robustness of control systems. Section 5 introduced sensitivity functions, crucial for designing weighting functions used in synthesizing $\mathcal{H}_\infty$ controllers, as detailed in Section 6. Section 7 provided an overview of PID robust control concepts, which will be expanded upon in Chapter 5. With these concepts in mind, Chapter 4 will delve into the design of two model-based $\mathcal{H}_\infty$ controllers.

3 MAIN CONTRIBUTIONS: ENHANCED ROBUST LATERAL $\mathcal{H}_\infty$ CONTROL SCHEMES

This Chapter details the student's main contributions to the VMC project, outlining the evolution of the control strategy from development to testing stages. The initial section provides an overview of $\mathcal{H}_\infty$ control, emphasizing the techniques and challenges employed within the project. The subsequent section delves into second $\mathcal{H}_\infty$ control scheme, summarizing both development and final results.

For the testing phase, the company provided scripts and Simulink models of the VMC project, which encompass all elements depicted in Figure 3. Additionally, a full vehicle model of a real Renault car was developed by the team, specifically the Renault Austral E-Tech, used for real tests. For high-level control, a PID controller with anti-wind-up and an associated lookup table was implemented. The only modification made in this dissertation pertains to the high-level control.

Considering that the vehicle's mass can vary significantly during operation due to factors like the number of passengers or luggage, a weight scale was used to measure the actual weight of a light vehicle (one passenger) and an overloaded vehicle (four passengers and bags). This approach evaluated the mass range to ensure the controller's robustness across various real-world scenarios, enhancing the overall effectiveness and safety of the VMC project.

Simulations were conducted under both nominal and adverse driving conditions to evaluate the performance of the proposed control scheme. Two control strategies were proposed: the first being standard $\mathcal{H}_\infty$ control and the second with modifications (confidential) into the synthesis process. The model used in both synthesis strategies considered a medium mass to ensure robustness for lower and higher masses and a medium velocity of 90 km/h as the operation point.

3.1 $\mathcal{H}_\infty$ CONTROL DESIGN

The $\mathcal{H}_\infty$ optimization problem seeks to minimize the $\mathcal{H}_\infty$ norm of the closed-loop transfer function from $w(t)$ to $z(t)$ is given as:

$$K(s) = arg \min_{K(s)} \| T_{zw}(s) \|_\infty \leq \gamma_\infty, \tag{33}$$

subject to:

$$P \rightarrow \left[\begin{array}{c} \dot{x} \\ \hline z \\ \hline y \end{array}\right] = \left[\begin{array}{c|cc} A & B_1 & B_2 \\ \hline C_1 & D_{11} & D_{12} \\ \hline C_2 & 0 & 0 \end{array}\right] \left[\begin{array}{c} x \\ \hline w \\ \hline u \end{array}\right], \tag{34}$$

where $w = [\dot{\psi}_{ref}, d]^T$ is the external input vector, $u = [M_z]$ represents the control input signals, $y = [\dot{\psi}]$ is the measured output, $z = [z_1, z_2]^T$ contains the weighted controlled

outputs and x is the state variables, defined as:

$$\begin{bmatrix} \dot{\beta} \\ \ddot{\psi} \end{bmatrix} = \begin{bmatrix} -\frac{C_f+C_r}{MV_x} & -\frac{C_f l_f - C_r l_r}{MV_x^2} - 1 \\ -\frac{C_f l_f - C_r l_r}{I_z} & -\frac{C_f l_f^2 + C_r l_r^2}{I_z V_x} \end{bmatrix} \begin{bmatrix} \beta \\ \dot{\psi} \end{bmatrix} + \begin{bmatrix} \frac{C_f}{MV_x} \\ \frac{l_f C_f}{I_z} \end{bmatrix} \delta_f + \begin{bmatrix} 0 \\ \frac{1}{I_z} \end{bmatrix} M_z. \tag{35}$$

For the $\mathcal{H}_\infty$ synthesis problem to be solvable, (A, B_2) must be stabilizable, which can be reached if for all eigenvalues λ_i of A such that $|\lambda_i| > 1$ holds and that:

$$rank \begin{bmatrix} (\lambda_i I - A) & B_2 \end{bmatrix} = n, \tag{36}$$

with I the identity matrix and n order of the system. Moreover (A, C_2) must be detectable, which can be reached if for all eigenvalues λ_i of A such that $|\lambda_i| > 1$ holds and that:

$$rank \begin{bmatrix} (\lambda_i I - A) \\ C_2 \end{bmatrix} = n. \tag{37}$$

Another crucial step in the control synthesis is the frequency analysis of the system, shown in Figure 9.

Figure 9 – Frequency response of the (linear) bicycle model.

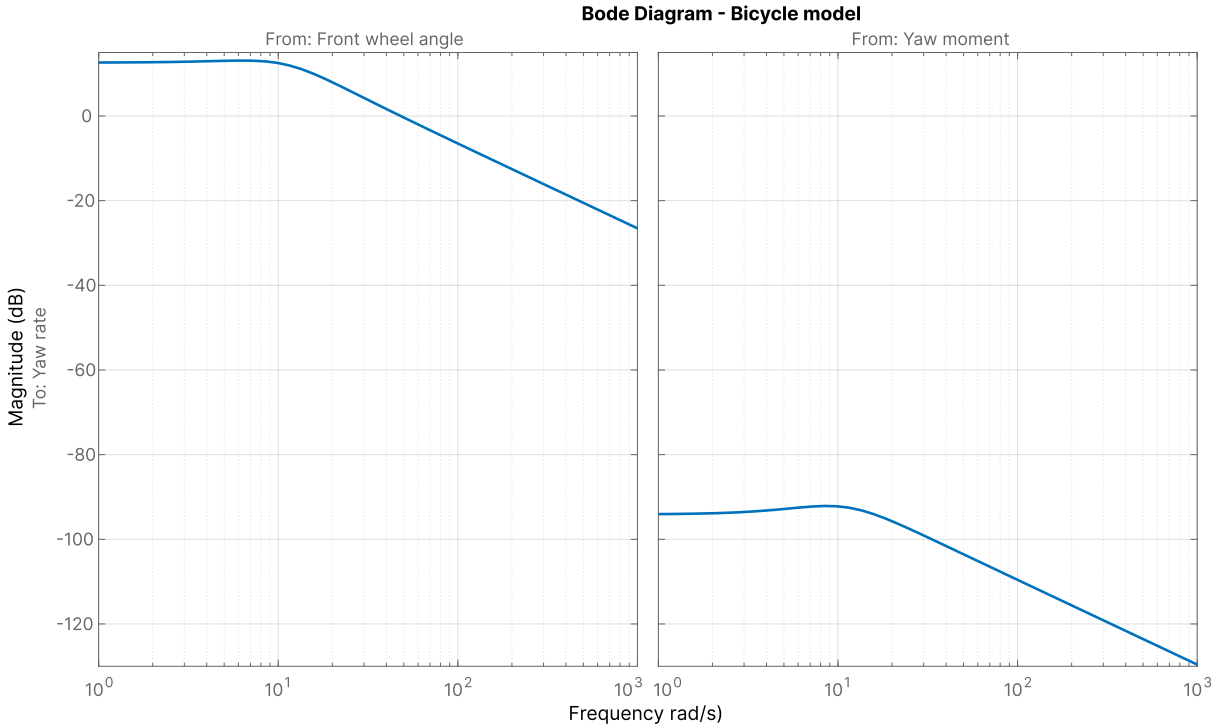

Source: The Author.

From the Bode diagram on the right side of Figure 9, it becomes evident that developing a frequency-based controller with yaw moment M_z as the control input presents an initial challenge. This is due to the notably low direct gain between the controlled variable $\dot{\psi}$ at low frequencies, impacting the overall gain of the open loop.

In practice, this would require a very high gain at low frequency for the error template $W_e(s)$ and a very low gain for the control template $W_u(s)$ to impose any performance. Additionally, there is limited literature on yaw rate control using M_z as the control input; most studies focus on using the front wheel angle δ_f. However, given that the vehicle is equipped with a yaw moment actuator and the dissertation is part of an ongoing project of over two years, it is not viable to change this aspect.

Attempts to develop control with M_z resulted in ineffective performance due to the frequency response, leading to sluggish and non-robust behavior. Consequently, a second strategy was explored. The solution involved emulating the control applied to δ_f, which has shown favorable results in existing literature (DOUMIATI, M. et al., 2010; YIN; CHEN, N.; LI, 2007). To accomplish this, the control signal was translated to δ_f and the templates enforced on this variable. It was then converted back into M_z before application to the real system. The initial step entailed restructuring the system as follows:

$$\dot{x} = Ax + B_1\ \delta_f + B_2\ M_z.$$

Subsequently, the control was designed using δ_f and applied to the system, with the generalized plant's actual output in terms of M_z. This translation necessitated ensuring the appropriate gain between them:

$$B_2\ M_z = B_1\ \delta_f.$$

Consequently:

$$\delta_f = [(B_1^\top\ B_1)^{-1}\ B_1^\top\ B_2]\ M_z,$$

where B_1 must have a rank such that the inverse $(B_1^\top B_1)^{-1}$ always exists. In other words, the columns of B_1 must be linearly independent, ensuring that $B_1^\top B_1$ is an invertible matrix. Resulting in a gain from M_z to δ_f of:

$$\delta_f = \left(-\frac{l_f\ m^2\ V_x^2}{l_z^2\ c_f + c_f\ l_f^2\ m^2\ V_x^2} \right)\ M_z. \tag{38}$$

In order to formulate the standard structure for the $\mathcal{H}_\infty$ controller defined in Figure 8, the weighting functions W_e, W_u and W_d are defined to characterize, respectively, the performance objectives, actuator limitations and disturbance rejection. Initial tests were performed using the bicycle model, followed by the VMC model to obtain optimal values in a more realistic scenario. The results differed due to the higher uncertainty and complexity of the full model. The bicycle model allowed for more demanding robustness and performance requirements, but the control proved unstable in the VMC due to delays and uncertainties. Therefore, the final values were chosen to balance robustness, performance and stability. The weight selection is summarized below, the values were kept confidential:

- Z_1 is the weighted yaw rate error output signal. It represents the yaw rate tracking performance. The corresponding weight W_e (29), where ω_S = x Hz is the cut-off frequency of the high pass filter, ϵ_0 = y is the attenuation level for low frequencies (f < ω_S). In this case y means that the static error must be lower than y%. And M_S = z is the maximum peak magnitude of the sensibility function S.
- Z_2 is the front wheel angle control signal attenuation. Its associate weight W_u (30), where ω_u = x Hz is the cut-off frequency of the low pass filter, ϵ_1 = y is the attenuation level for high frequencies (f > ω_u) and M_u = z is the actuator saturation.
- d is the disturbance. Its associate weight W_d is a simple gain of x, which will impact in the sensitivity functions $T(s)$ and $S(s)G(s)$.

These weighting functions are reflected in the sensitivity function plots as upper bound limits, i.e. W_i^{-1}.

In practice, designing a mixed-sensitivity controller for the plant, augmented by loop-shaping filters, involves defining the plant, weighting filters and augmented plant using Simulink or the YALMIP toolbox (LOFBERG, 2004). The controller is synthesized using the MATLAB function `hinfsyn`, which employs the Riccati method by default to solve the optimization problem. This function takes as input the number of measurement outputs and control inputs and provides as output the controller K, the closed-loop transfer function CL, both as continuous state-space models and the performance level γ used to compute the controller K.

Following these steps, a generalized plant P was found with 3 outputs, 3 inputs and 4 states, and a controller K with 1 output, 1 input and 4 states. The resulting open loop frequency response is keep confidential.

Regarding the performance and robustness of the controller, the optimization problem yielded an optimal gain γ of 0.89, which is an almost optimal result. Ideally, it should be equal to 1, but a compromise was made between performance, robustness and stability, limiting γ to ensure optimal results.

3.1.1 Simulation in VMC project

For implementation in the VMC project, it was necessary to discretize the controller since the project operates in discrete time, a sampling time of $t_s = 0.01s$ was used. In the simulation, various parameters can be set to define different vehicle dynamics, with the most relevant to the control scheme being the mode and the weight on the control allocation. For these tests, the mode was set to "normal". Regarding the weight, it was recommended to use a higher weight for a lower μ, prioritizing braking over steering. This strategy, based on tests in the real vehicle, proved to be more stable for

the current control scheme, leading to its continued use in the new High-Level control. Additionally, during the tests, it is possible to change the vehicle mass within the vehicle model's subsystem. This ensures that the reference model remains unaware of the mass change, thereby simulating real-life conditions where there is no mass estimation to inform the reference model.

The first simulation it was set a medium mass and the pilot's inputs, steering angle as in Figure 10 and longitudinal velocity V_X = 90 km/h and road conditions, tire/road contact friction coefficient μ = 1.

Figure 10 – Pilot's input.

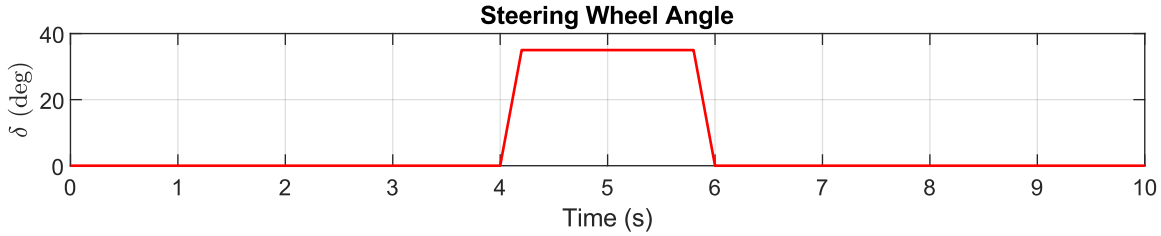

Source: The Author.

During the tests, an overshoot in the response was observed, which contradicted the analysis of the sensitivity function T. This discrepancy suggests that the dynamics of the real vehicle are faster than those predicted by the simplified bicycle model. After further analysis, it was determined that the controller did not handle sudden changes in references well. To address this issue, a second-order filter was added to smooth the reference signal. This change eliminated the overshoot in the controller's response.

The second-order filter is defined by:

$$\frac{1}{1 + \left(\frac{2\xi}{\omega}\right) s + \frac{s^2}{\omega^2}}, \tag{39}$$

with ξ = 1.5 and ω = 70 Hz.

Figure 11 shows a comparison of the control response with (depicted in green) and without the filter (blue) and the reference (red).

Figure 11 – Comparison yaw rate control with filter and without it - medium mass.

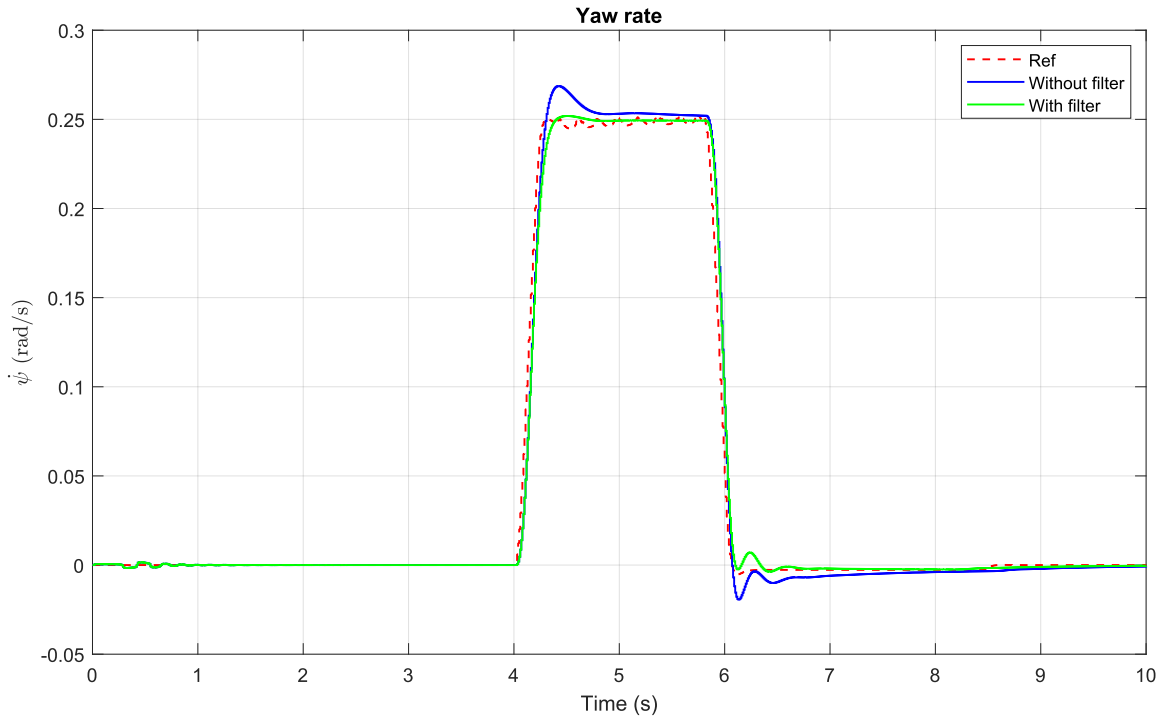

Source: The Author.

Since the filter significantly reduced the overshoot without introducing delay, it was included in the reference for subsequent tests.

To evaluate the effects of the VMC project with the $\mathcal{H}_\infty$ control, tests were conducted both with and without VMC. The pilot's inputs are, δ as in Figure 12 and V_X = 90 km/h and road conditions, μ = 1 with a medium vehicle mass.

Figure 12 – Pilot's inputs.

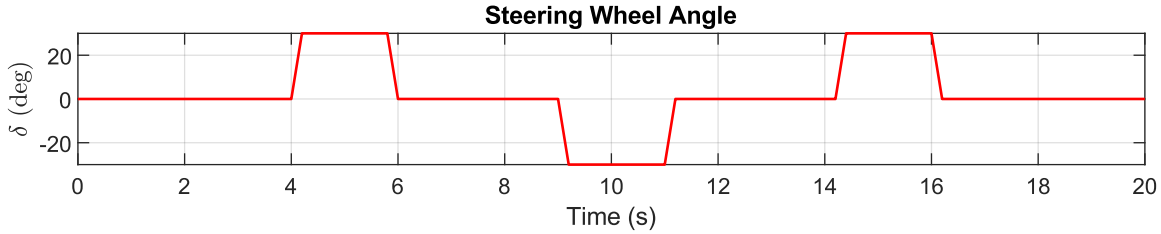

Source: The Author.

This configuration results in a maximum lateral acceleration of 5.6326 m/s^2.

Figure 13 – Comparison yaw rate control with VMC and without it - medium mass.

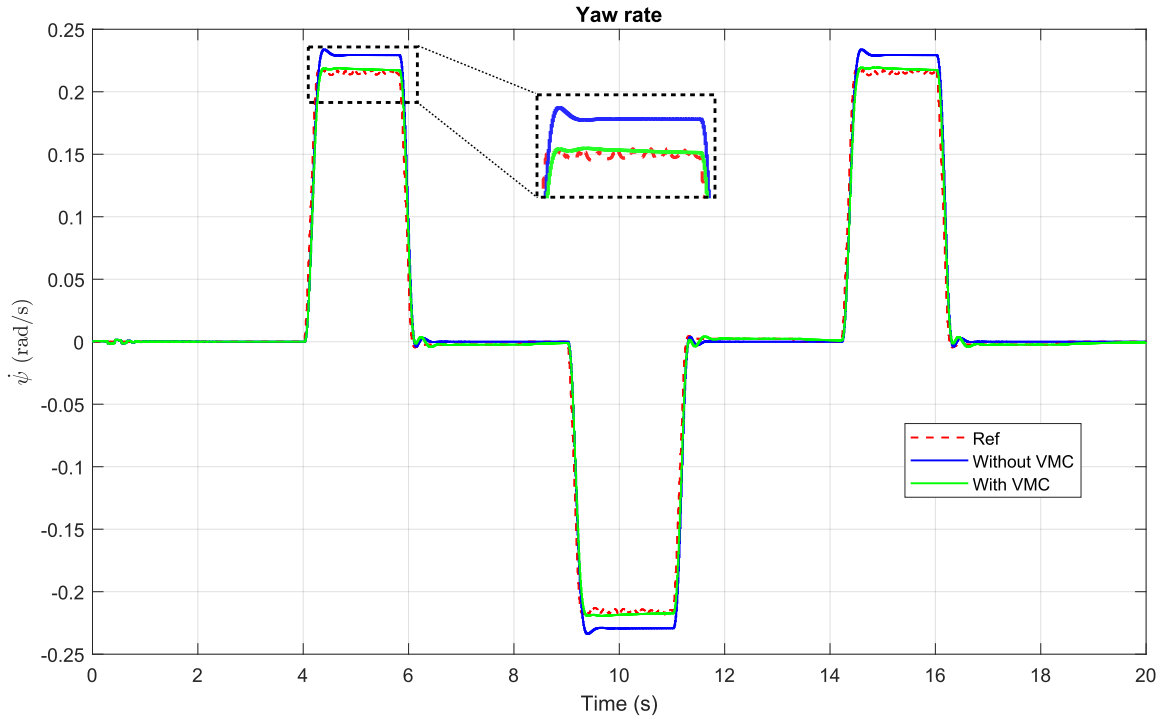

Source: The Author.

As shown in Figure 13, the yaw rate with VMC (depicted in green) demonstrates better reference (red) tracking compared to the scenario without it (blue). This highlights the improved performance and stability provided by the project.

Another important variable that is directly impacted by the performance of the project is the vehicle's position, since the primary objective of the project is to ensure that the vehicle can successfully follow a trajectory without excessive oversteer or understeer.

Figure 14 – Comparison vehicle's position with VMC and without it - medium mass.

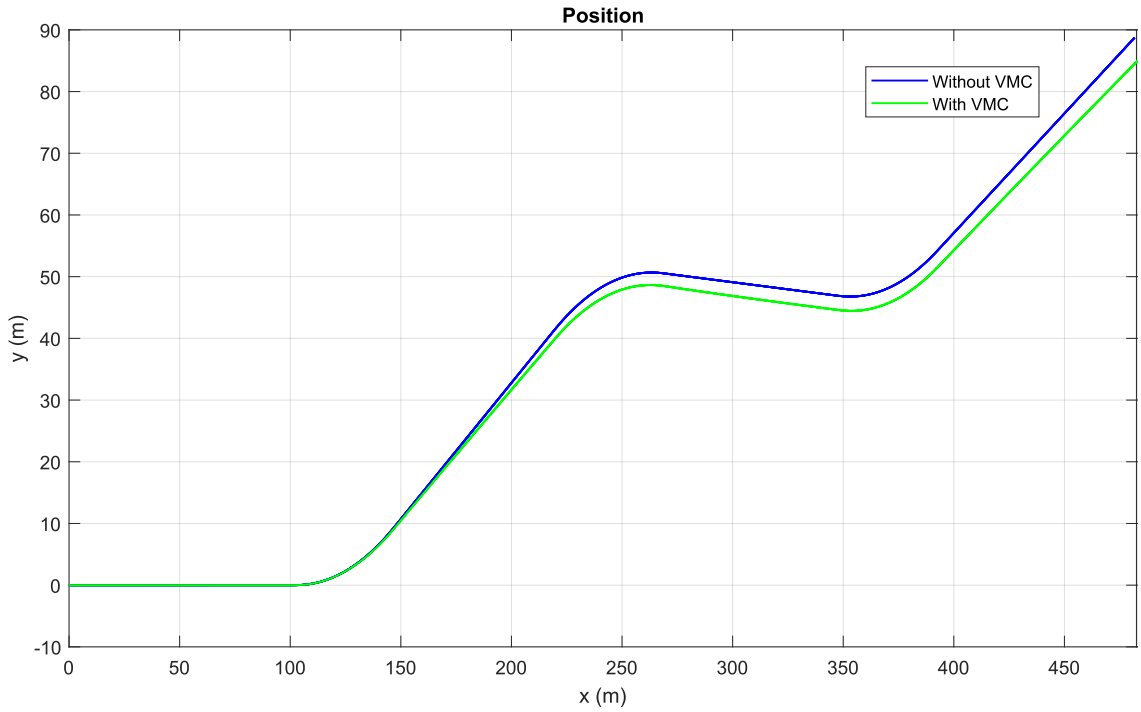

Source: The Author.

Figure 14 shows a comparison of the vehicle's position with and without VMC. As expected, the vehicle equipped with the VMC performs the maneuver with a narrower curve, resulting in a distance of two meters between the trajectories. This demonstrates the effectiveness of the VMC system in maintaining the desired path and improving overall trajectory tracking.

To meet the company's request for robustness, particularly concerning variations in vehicle mass and different road adhesion conditions, tests were conducted. Using the same input as shown in Figure 12, but with a focus on evaluating the robustness of the vehicle.

Figure 15 – Comparison yaw rate control - low, medium and high mass.

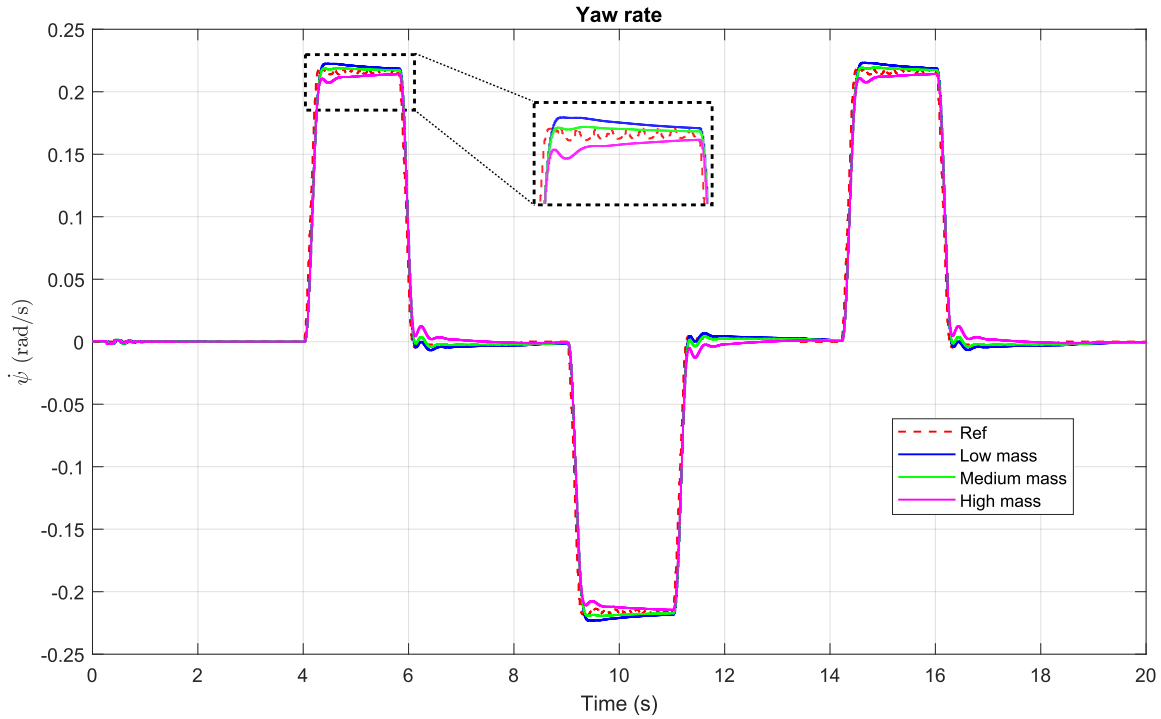

Source: The Author.

In Figure 15, the reference trajectory (depicted in red) is compared with the yaw rates corresponding to low (blue), medium (green) and high (pink) vehicle masses. This comparison highlights the controller's consistent performance across different mass configurations, affirming its robustness in accommodating variations in vehicle dynamic.

Figure 16 – Comparison yaw Moment - low, medium and high mass.

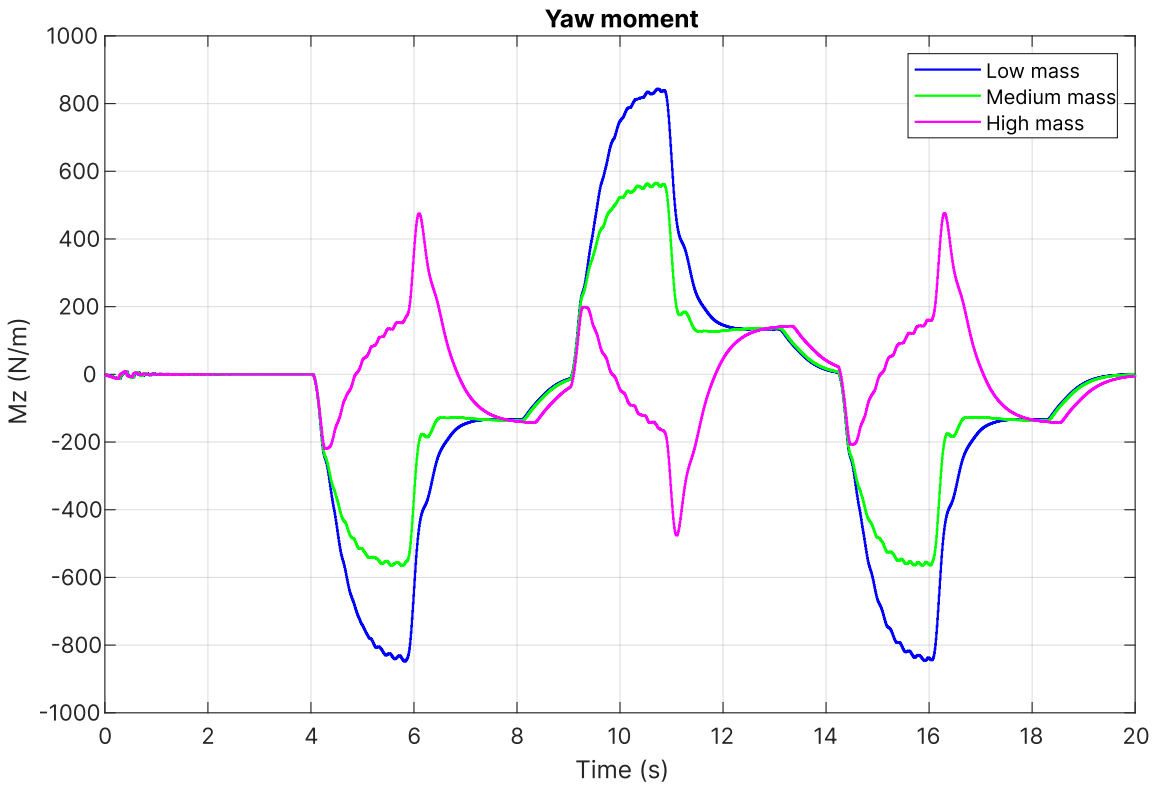

Source: The Author.

In Figure 16, it is observed that even when the reference is set to zero, the control input does not return to zero. This issue originates from the reference model, which is still in development. Although this problem was not apparent with the PID controller, the $\mathcal{H}_\infty$ controller, which closely follows the reference, revealed the issue. After making the necessary changes, the yaw rate control remained the same, as shown in Figure 15. However, the yaw moment changed as follows:

Figure 17 – Comparison yaw moment - low, medium and high mass.

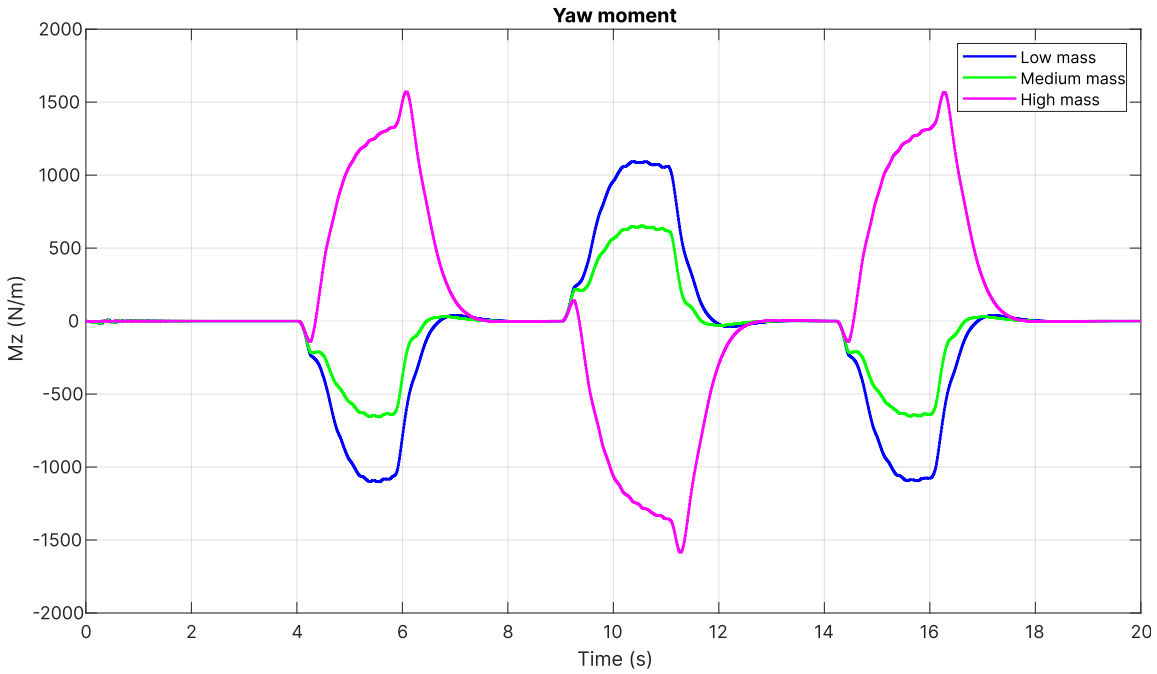

Source: The Author.

In Figure 17, the shape and magnitude of the yaw moment vary according to the vehicle's mass, reflecting changes in the dynamics. For a higher mass, the yaw moment aligns with the yaw rate reference (positive or negative) because the increased moment of inertia requires a higher torque to achieve the same angular acceleration.

3.1.2 Tests in the real vehicle

The prototype vehicle is equipped with a MicroAutobox, an embedded PC platform capable of reading sensor data and sending signals to the vehicle's actuators. To implement the project within this environment, it was necessary to translate the Matlab/Simulink code to C and then compile it into the Microbox. Another necessary modification for the testing was the addition of a switch, ensuring that the controller would only be activated for longitudinal velocities greater than 30 km/h.

The tests were conducted at Renault's testing center, which features various tracks, allowing the vehicle to be tested under different road conditions and maneuvers. During the tests, a test driver drove the vehicle with the student supervisor and the student onboard, so configuration a medium mass in the vehicle.

As soon as the control system was activated in the vehicle, it was evident that the controller was very strong. Therefore, the pilot decided to not continue to the track. Although, the controller described in the next Section underwent rigorous testing in various conditions and on different types of roads.

3.2 SECOND $\mathcal{H}_\infty$ CONTROLLER SCHEME DESIGN

To remain confidential - control under patenting process.

3.2.1 Tests in the real vehicle

In this subsection, three selected tests will be presented. All three were conducted in the vehicle with three occupants, representing a medium load. Three different tracks were used for each test:

1. City Circuit: As the name suggests, this track simulates an urban environment with typical "soft" curves and a roundabout. It is designed to represent normal city driving conditions.
2. Mountain Circuit: This track represents an ascending and descending road with tighter curves, similar to those found on a mountain road. It is more demanding than the city circuit but still represents a common driving scenario.
3. Handling Track: This track is more akin to a race track, used to test high-speed driving with narrow curves. It is the most demanding of the three in terms of control.

These circuits are arranged in ascending order of control demand. The first test was conducted on the city circuit to evaluate the stability and performance of the controller at low speeds, ensuring it is stable enough for more challenging scenarios. The layout of the first test circuit is shown in Figure 18, where the x marks the starting point of the trajectory.

Figure 18 – City circuit

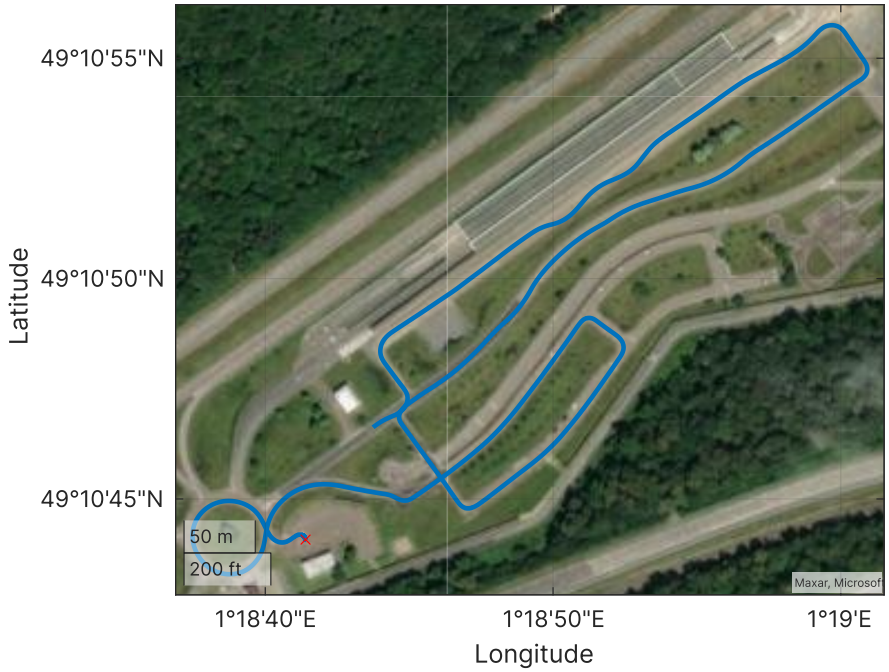

Source: The Author.

On the testing day, it was raining, which theoretically lowered the coefficient of adhesion μ below 1. However, for this initial test, within the VMC model (control allocation and reference model), μ was maintained at 1, as the $\mathcal{H}_\infty$ control demonstrated greater stability under this condition. The vehicle was also tested in normal driving mode.

Figure 19 – Pilot's inputs - city circuit

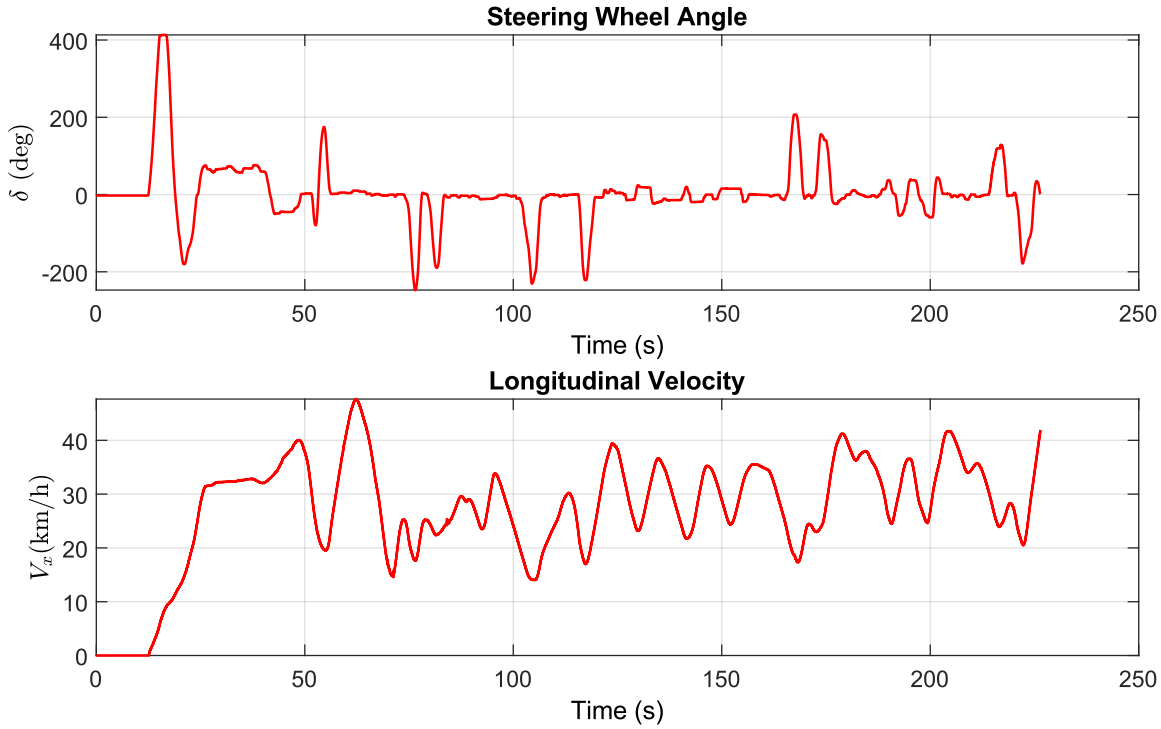

Source: The Author.

In Figure 19, the pilot's inputs, steering wheel angle and longitudinal velocity are displayed. These inputs generated the resulting yaw rate control.

Figure 20 – Yaw rate control - city circuit

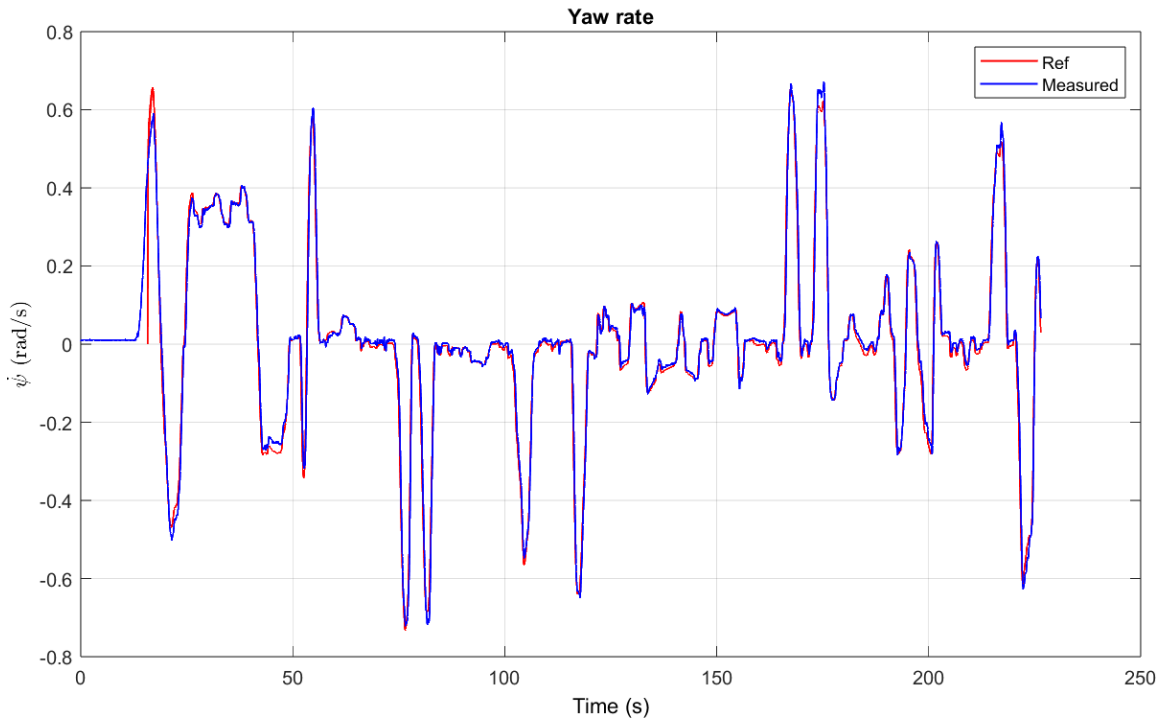

Source: The Author.

As shown in Figure 20, the control system performed very well, resulting in a Root Mean Square (RMS) value of the error $(\dot{\psi}(t) - \dot{\psi}_{ref}(t))$ equal to 0.0366, what indicates good tracking. The pilot commented that he could feel the control system assisting him during the curves. Given the successful performance of the control system, the complexity of the tests was subsequently increased.

For the next test, the high μ configuration was maintained. To evaluate the control system's robustness under different setups, the driving mode was switched to sport, resulting in more agile vehicle dynamics.

Figure 21 – Mountain circuit

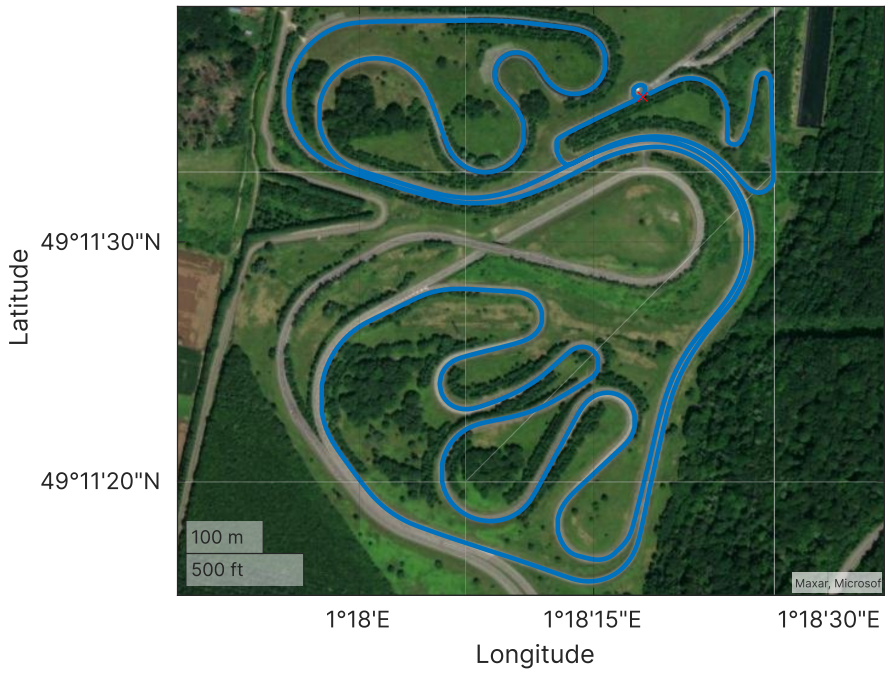

Source: The Author.

The circuit displayed in Figure 21 represents a mountain route, featuring slopes and narrow curves.

Figure 22 – Pilot's input - mountain circuit

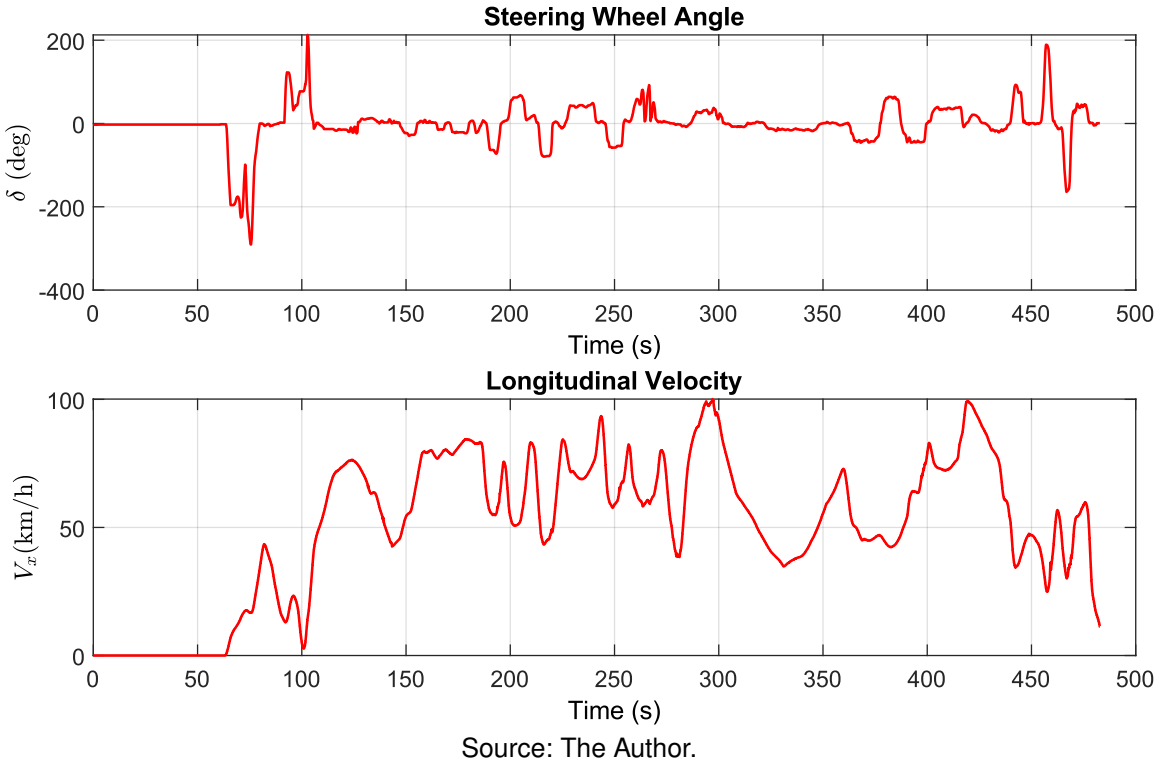

Source: The Author.

In Figure 22, the pilot's input, steering wheel angle and longitudinal velocity are displayed, reaching a maximum velocity of 100 km/h. The controlled variable is shown in Figure 23.

Figure 23 – Yaw rate control - mountain circuit

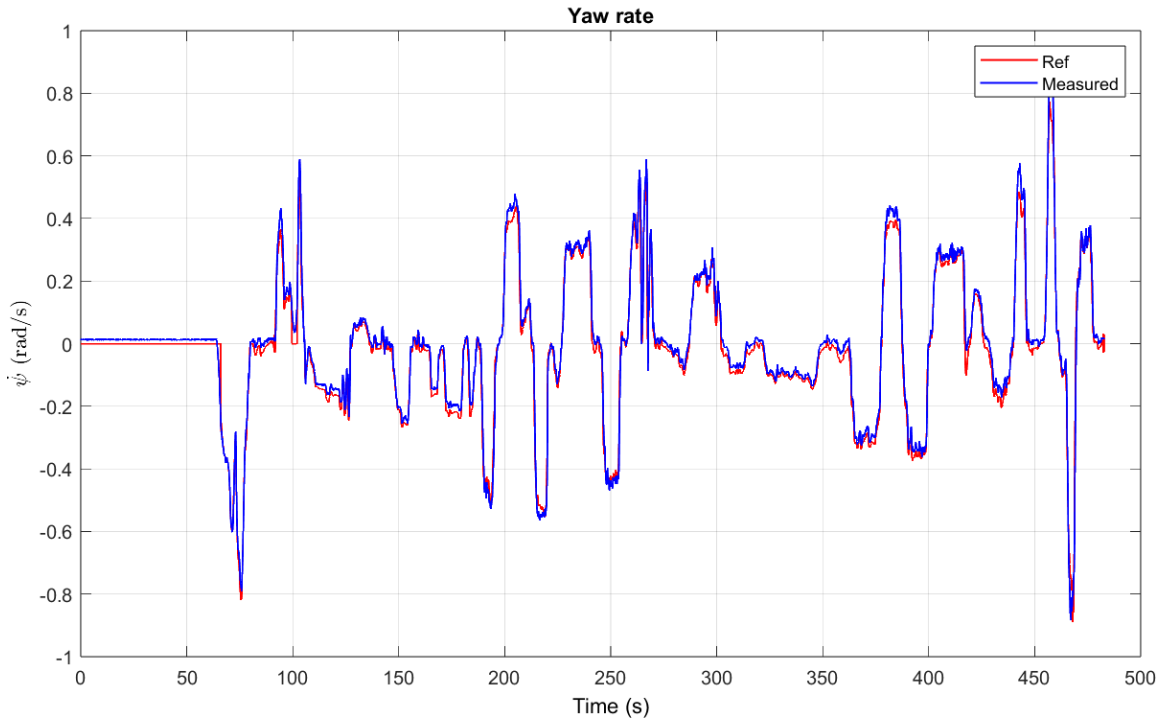

Source: The Author.

In Figure 23, the control system demonstrates good tracking performance, even on a more challenging mountain circuit, with an RMS error of 0.0316. The pilot noted that the control felt strong, statement confirmed by analyzing the outputs of the VMC project.

Figure 24 – Output VMC - mountain circuit

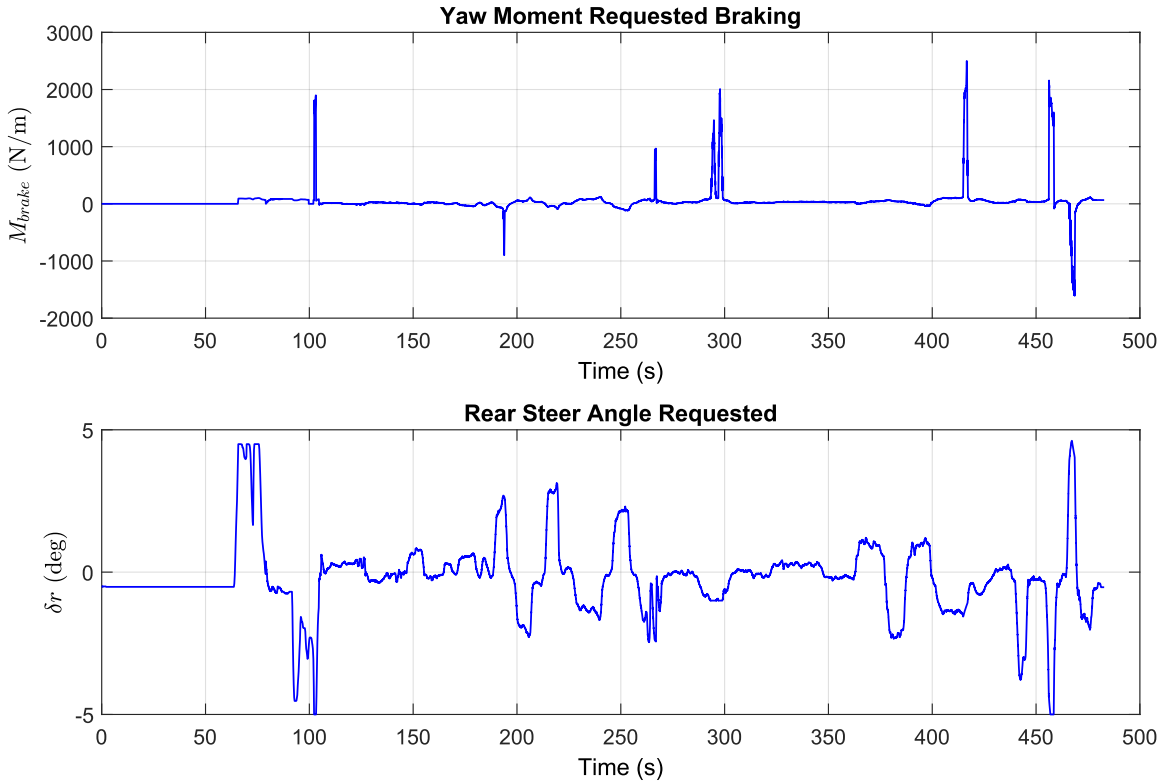

Source: The Author.

In Figure 24, the yaw moment braking and rear steer angle, both signals sent from the VMC to the vehicle, are depicted. While some oscillations are noticeable in both signals, they did not induce discomfort inside the vehicle. Additionally, abrupt changes are observed in both signals, particularly pronounced in M_{brake} , which shifts from 0 to nearly 2000 N/m in less than 10 seconds. Another point noted was that after navigating narrow curves, the steering wheel was visually shifted a few degrees from the 'neutral' state. Occasionally, the steering wheel returned to its original position, but in other instances, it remained shifted. This phenomenon is evident at the 350-second mark, where the yaw rate target (Figure 23) is null, so the rear steer angle should also be null, however, this is not the case. This issue was also observed during the simulation phase, as mentioned in previous sections and was resolved by changing the reference model. The discovery of this solution, though, came after the tests in the vehicle.

The third test was conducted on a handling track, which is commonly used to explore the nonlinear zone of tire behavior. In this zone, the lateral tire forces do not depend linearly on the tire sideslip angle, as assumed in the bicycle model used in the synthesis of the controller. This test is also used to analyze vehicle behavior during cornering maneuvers and to assess overall vehicle dynamics. During this test, the vehicle was driven at high speeds, deliberately navigating narrow curves and inducing

abrupt changes in the steering wheel angle. The control allocation and reference model were set for a high μ configuration and the driving mode set to normal. From $t = 0\,\text{s}$ to $t = 160\,\text{s}$, the vehicle completes the first lap, after it follows the second lap follows, pushing more the vehicle to its limits on the track.

Figure 25 – Handling track

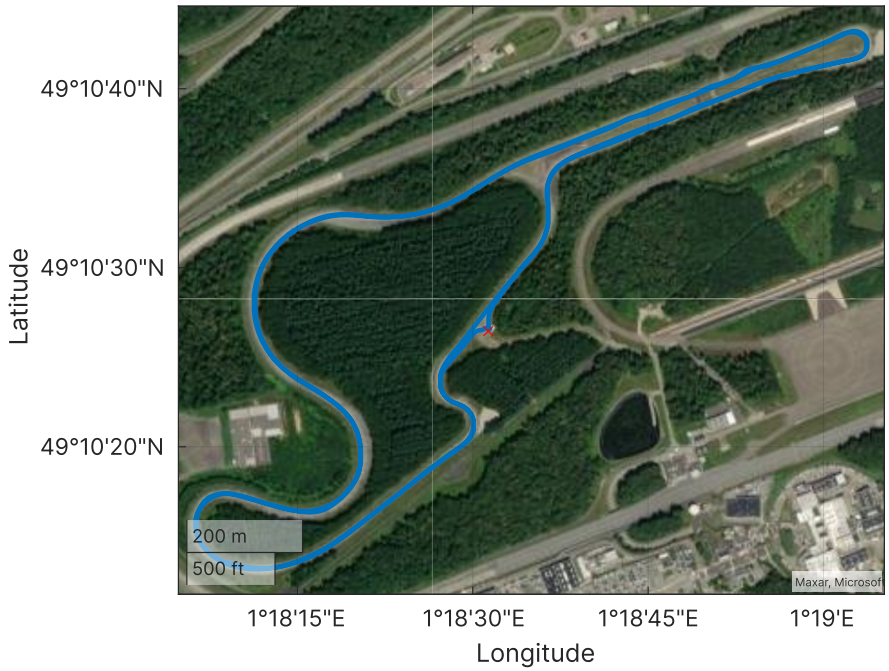

Source: The Author.

The pilot's input can be seen in Figure 26.

Figure 26 – Pilot's input - handling track

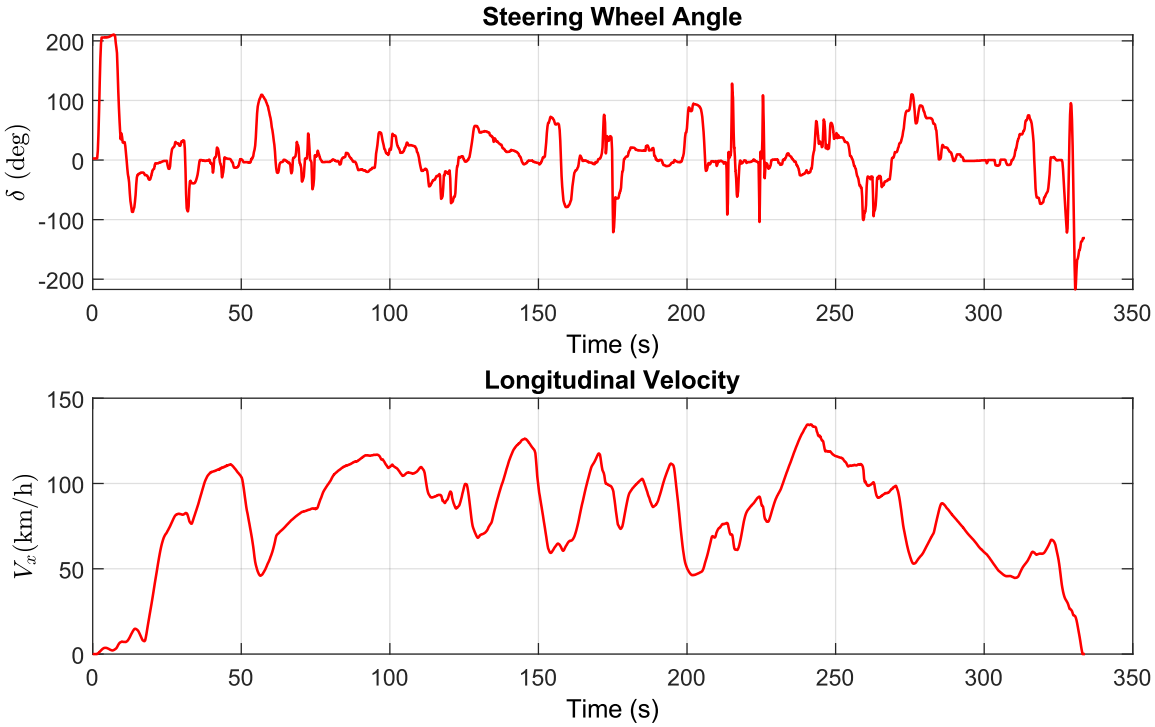

Source: The Author.

In Figure 26, the profile of the pilot's input is noticeably more demanding than in the previous two tests. For example, between 210 s and 230 s, the pilot made rapid left and right movements with the steering wheel. From 240 s to 250 s, the pilot accelerated the vehicle up to 135 km/h while aggressively steering, attempting to push the control system to its limits. The yaw rate resulting is presented in Figure 27.

Figure 27 – Yaw rate control - handling track

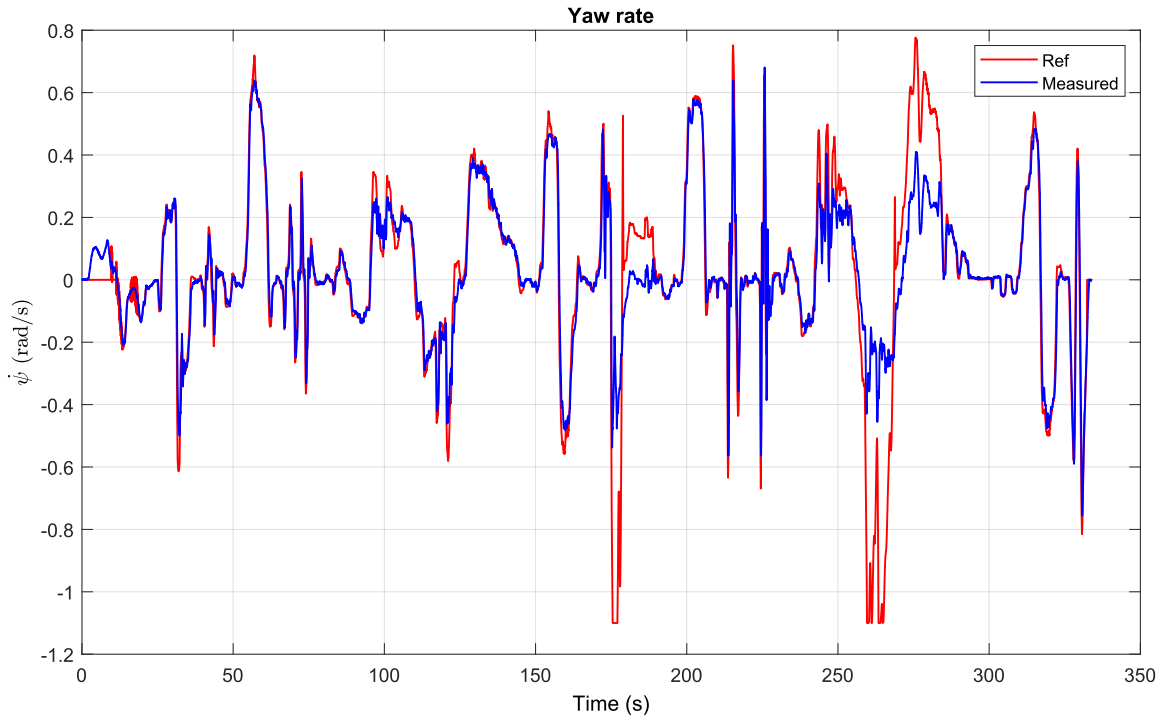

Source: The Author.

In Figure 27, the limitations of the control system are evident as it struggles to match the yaw rate reference in the second lap (t = [160, 330]s). Despite the intensity of the test, overall, the control demonstrated good performance. However, a notable observation, consistent with previous tests, is that the $\mathcal{H}_\infty$ controller generates a significantly high yaw moment, which is then transmitted to the outputs of the VMC project. This results in more pronounced braking and steering actions than expected. While these actions do not destabilize the vehicle, they are notably more aggressive compared to those of the current PID controller. In Figure 28, the behavior of the yaw moment control can be observed.

Figure 28 – Yaw moment - handling track

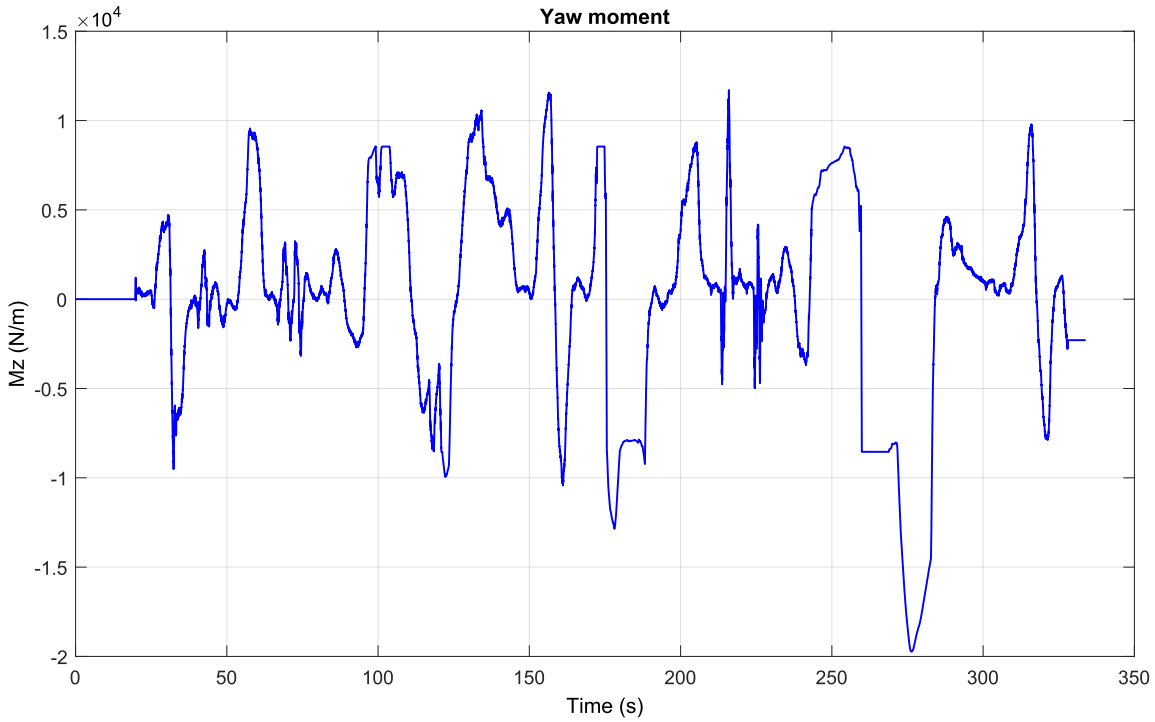

Source: The Author.

In Figure 28, the illustration depicts how the controller reacts to different conditions and inputs. The magnitude of the control action is evident. The oscillations observed in simulations for this controller were absent even during the most challenging test conditions.

It is worth noting that the $\mathcal{H}_\infty$ controller used in the tests employed the same weighting functions as the one used in the simulation, which yielded promising results. Despite some imperfections to be fixed, tuning the controller entirely in MATLAB proved to be a fast and efficient method, unlike PID controllers that typically require extensive real-world testing for fine-tuning.

To conclude this section, one key issues emerged from both simulation and real vehicle tests: the aggressive nature of the control inputs. Despite this downside, both $\mathcal{H}_\infty$ controllers demonstrated robust performance in simulation, showcasing robustness against variations in mass and various levels of μ. Both also delivered strong performance across all three driving modes.

However, it was observed that only the second controller achieved satisfactory results during physical tests. To assess whether these performances warrant replacing the current PID controller, the following section will conduct a comparative analysis of both control strategies.

3.3 COMPARISON BETWEEN ONBOARD PID AND PROPOSED SCHEME

As previously discussed, the yaw rate control in the VMC project uses a PID controller with an anti-windup technique, tuned using a lookup table. The lookup table adjusts according to the longitudinal velocity V_x and lateral acceleration a_y. The $\mathcal{H}_\infty$ controller was designed for a longitudinal velocity V_x of 90 km/h. Consequently, the frequency analysis of the PID was conducted for all lateral acceleration points in the lookup table, based on the system with Mz as control input. The open-loop frequency response plot and explanation are kept confidential.

To compare both control methods (PID and second $\mathcal{H}_\infty$ controller), a more dynamic reference is used, which includes varying velocity and steering angle as displayed in Figure 29 and $\mu = 1$.

Figure 29 – Pilot's input

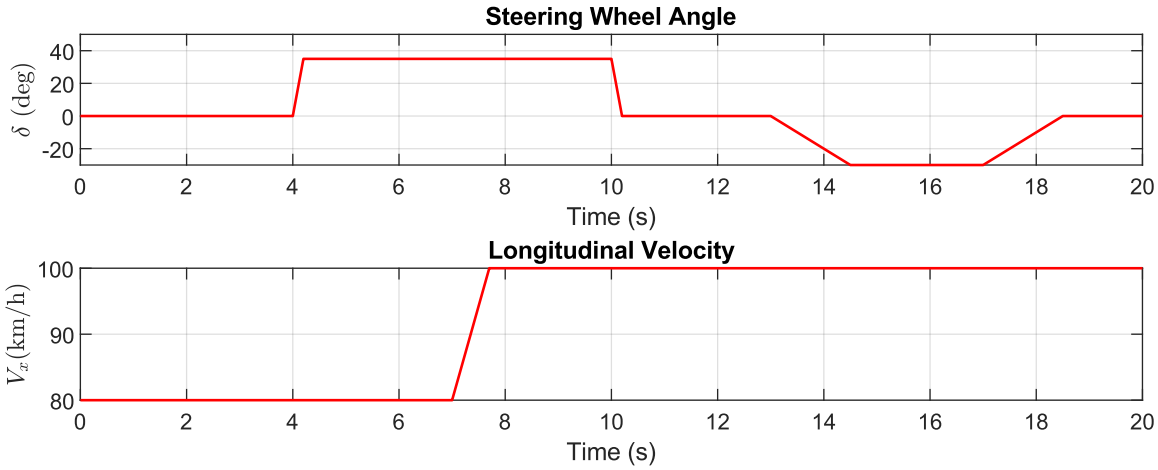

Source: The Author.

The yaw rate comparison is shown in Figure 30.

Figure 30 – Comparison yaw rate control PID and $\mathcal{H}_\infty$ controllers - varying mass.

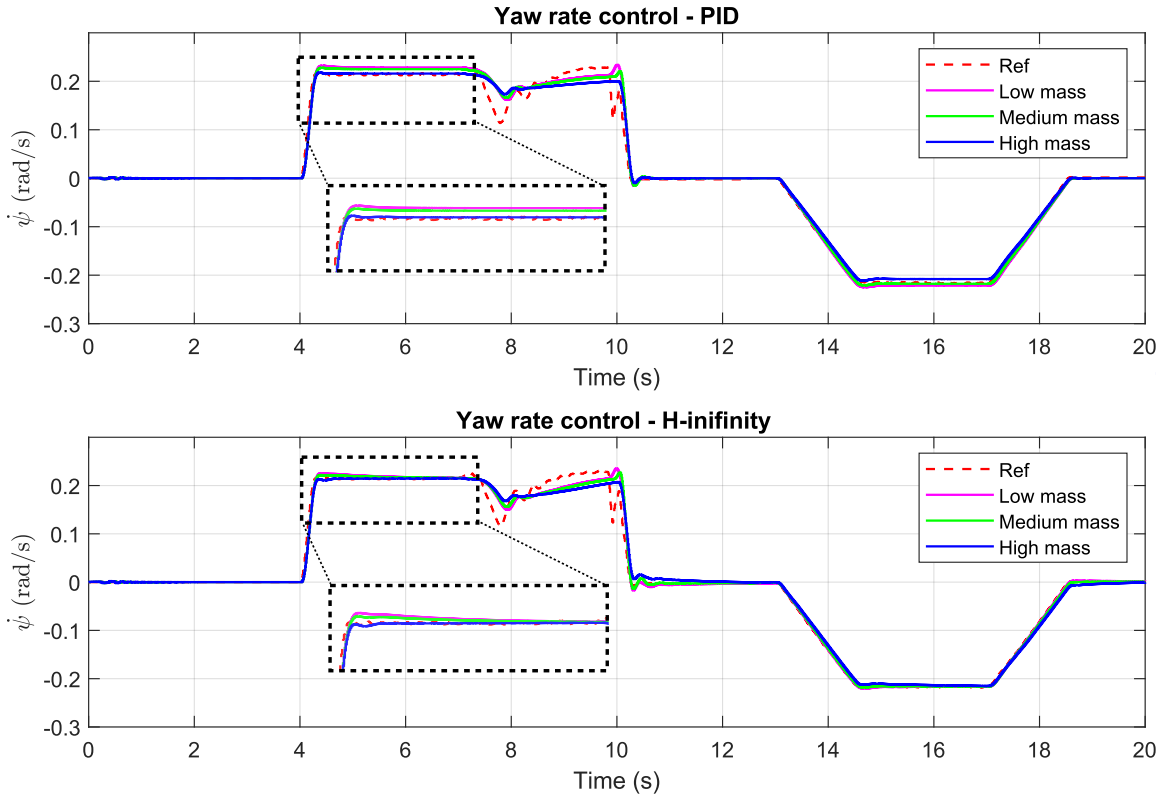

Source: The Author.

An improvement in robustness regarding mass can be observed. However, when the reference returns to zero, the PID controller responds faster than the $\mathcal{H}_\infty$ controller. For a more concrete comparison, the RMS value of the error $(\dot{\psi}(t) - \dot{\psi}_{ref}(t))$ is presented in Table 1, where a value close to zero indicates good tracking.

	PID	$\mathcal{H}_\infty$
Low mass	0.014	0.013
Medium mass	0.013	0.013
High mass	0.010	0.009
Average	0.012	0.011

Table 1 – Comparison of RMS of the tracking error PID and $\mathcal{H}_\infty$

Upon evaluating the values, both controllers demonstrate results close to zero. Furthermore, the $\mathcal{H}_\infty$ controller exhibits a smaller error for both low and high mass scenarios, representing an improvement of only 0.001 in robustness for this scenario. To determine if this enhancement in robustness justifies the trade-off, it is essential to analyze the control input displayed in Figure 31.

Figure 31 – Comparison yaw moment PID and $\mathcal{H}_\infty$ controllers - varying mass.

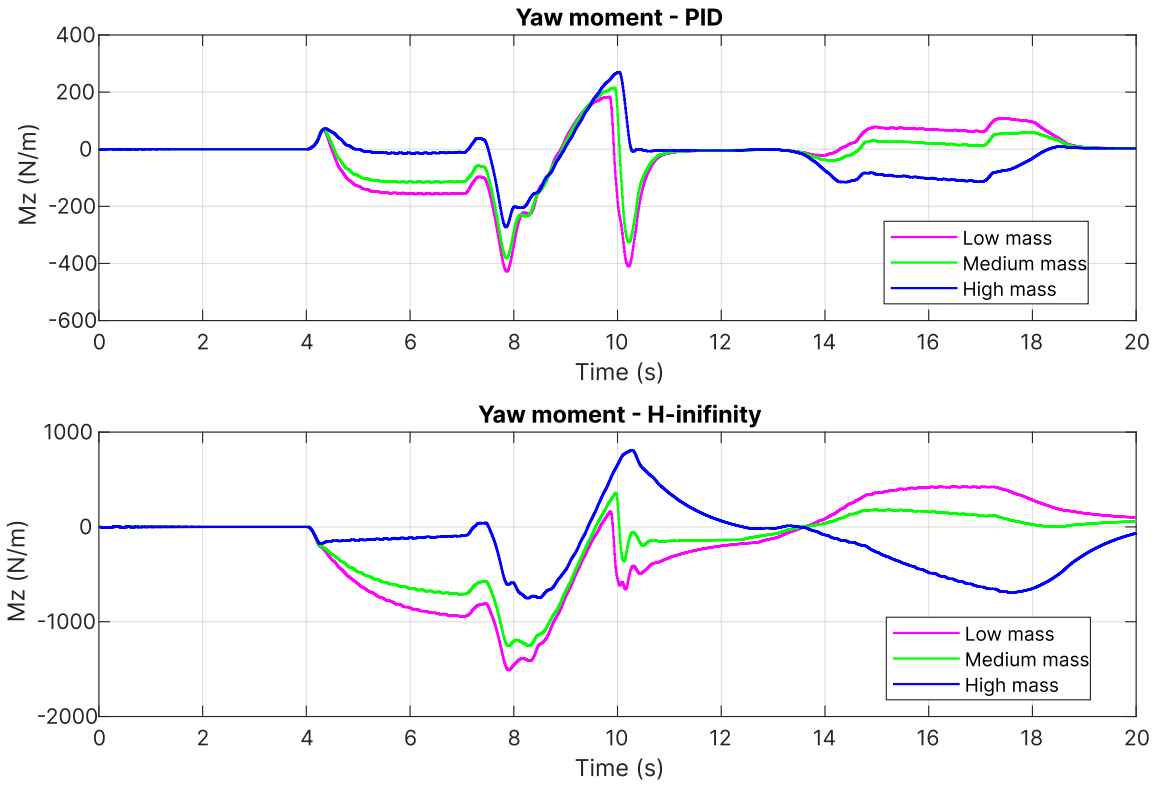

Source: The Author.

In order to analyse the power of the control, it can be calculated the total variance of the control signal (VT) given by the integral of the difference of two subsequent samples of $u(t)$, such as:

$$\int_1^t |M_z(\tau) - M_z(\tau - 1)| d\tau \tag{40}$$

For this metric, a higher value represents a more variant control input, consequently more aggressive.

	PID	$\mathcal{H}_\infty$
Low mass	3.166	74.574
Medium mass	3.134	89.224
High mass	3.044	83.056
Average	3.115	82.285

Table 2 – Comparison of total variance of the control input PID and $\mathcal{H}_\infty$

From this comparison, it becomes evident that the control input is significantly more potent with the $\mathcal{H}_\infty$ controller compared to the PID controller. Attempts were made to implement various weighting functions for the control input in order to mitigate its strength. However, as these adjustments were made, the robustness of the system also decreased. The results presented here represent the optimal balance between robustness and control power achieved by the controller. One hypothesis for this

observation is that the translation method used in the synthesis process attempts to implement control in a system with very low gain. Additionally, since the robust control is synthesized to include the worst-case gain, it is expected to be stronger than the PID controller.

Next, the system was tested using a medium mass and the control allocation gain was adjusted to prioritize braking more than in the previous setup. This adjustment was made for the next evaluation, considering μ = 0.7, characterizing a 'light' rain, V_x = 80 km/h and δ as in Figure 32.

Figure 32 – Pilot's input and road conditions.

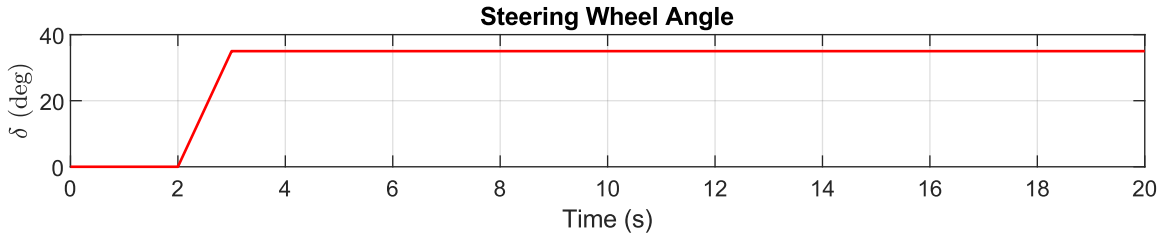

Source: The Author.

This reference categories a constant turn in the steering wheel. In Figure 33 the result of the controlled variable is displayed.

Figure 33 – Comparison yaw rate control PID and $\mathcal{H}_\infty$ controllers - medium mass and μ = 0.7.

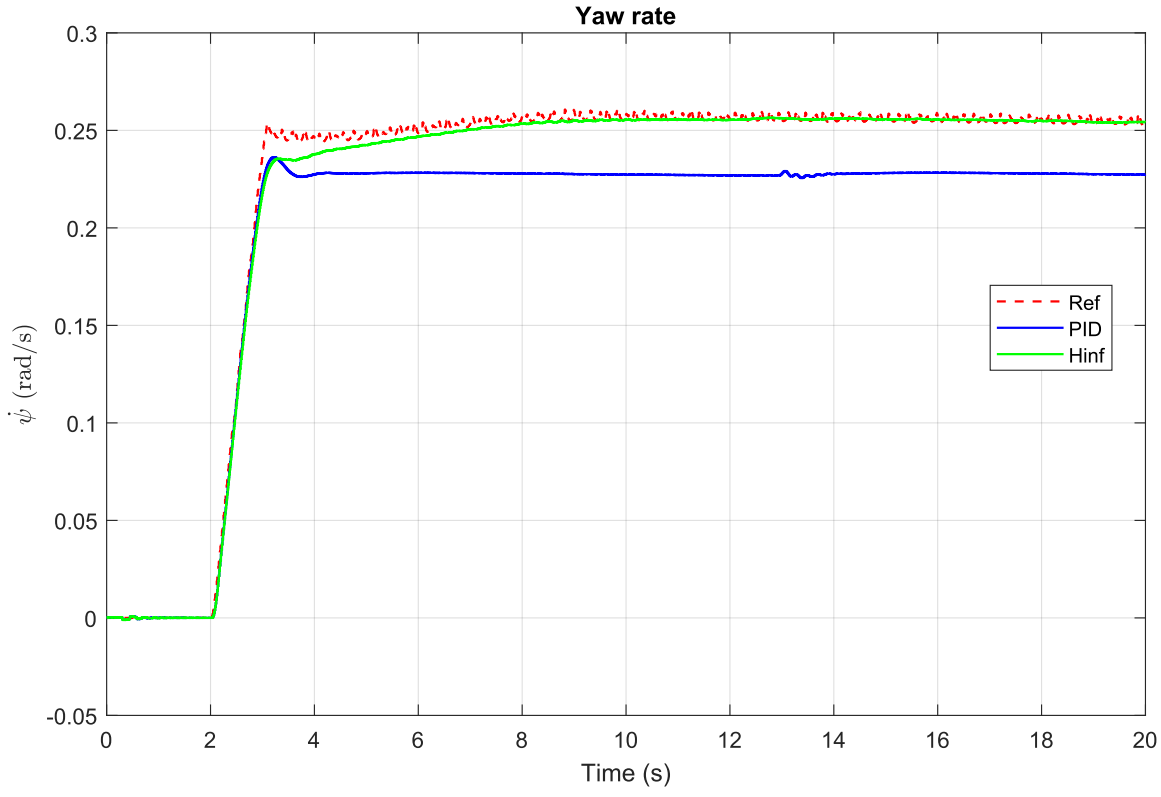

Source: The Author.

In this scenario, the PID controller fails to reach the reference, indicating that the lookup table is insufficient to ensure robustness under these conditions. However, due to the adaptability of the $\mathcal{H}_\infty$ controller, it successfully brings the yaw rate to the reference. Comparing the RMS of the tracking error presented in Table 3.

PID	$\mathcal{H}_\infty$
0.021	0.003

Table 3 – Comparison of RMS of the tracking error PID and $\mathcal{H}_\infty$

The $\mathcal{H}_\infty$ control demonstrates better tracking performance compared to the PID controller. As a result, the vehicle is capable of executing sharper turns, as evidenced in Figure 34.

Figure 34 – Comparison position PID and $\mathcal{H}_\infty$ controllers - medium mass and μ = 0.7.

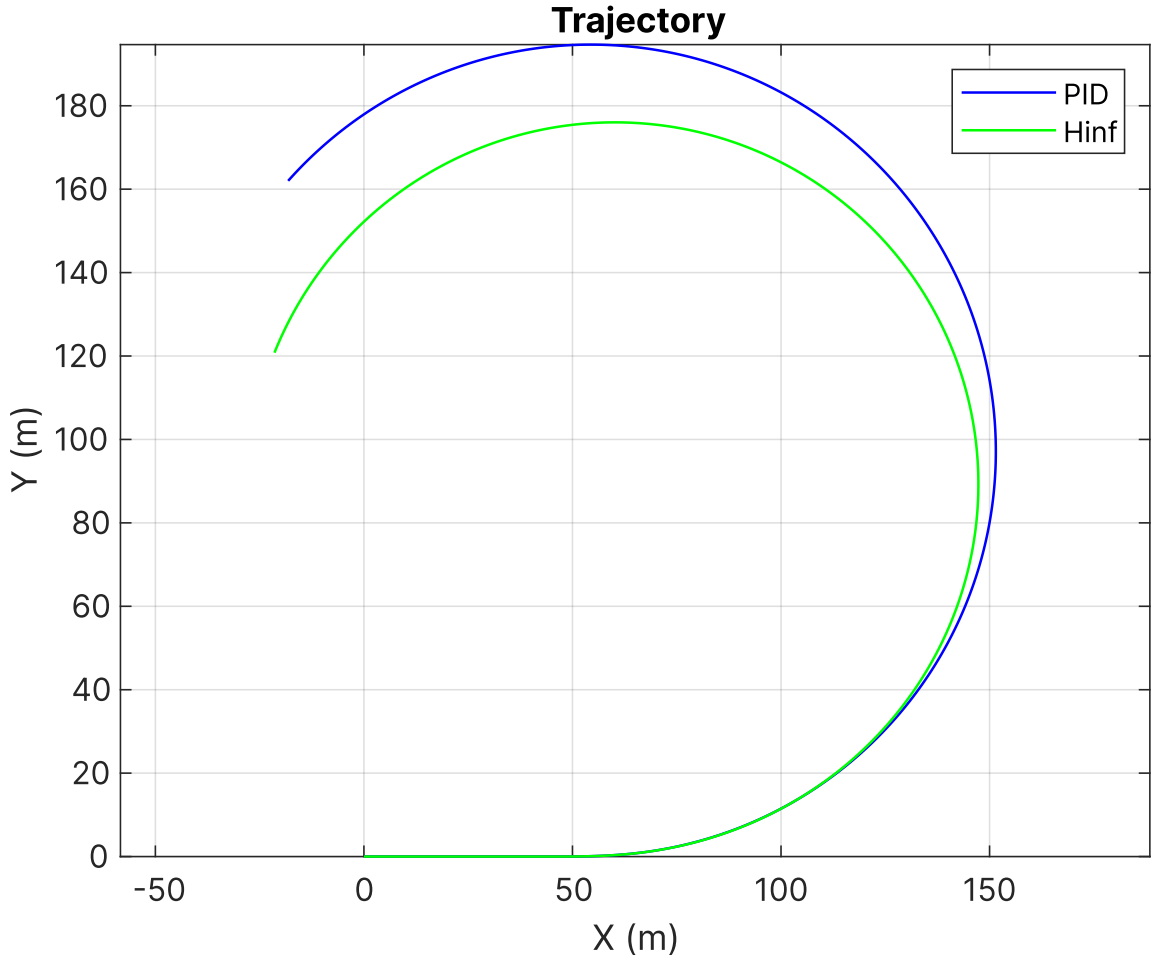

Source: The Author.

In Figure 34, the simulation with $\mathcal{H}_\infty$ controller demonstrates less sliding of the vehicle compared to the PID controller. As observed in Figure 35, this enhancement in performance is not without trade-offs.

Figure 35 – Comparison output VMC PID and $\mathcal{H}_\infty$ controllers - medium mass and $\mu = 0.7$.

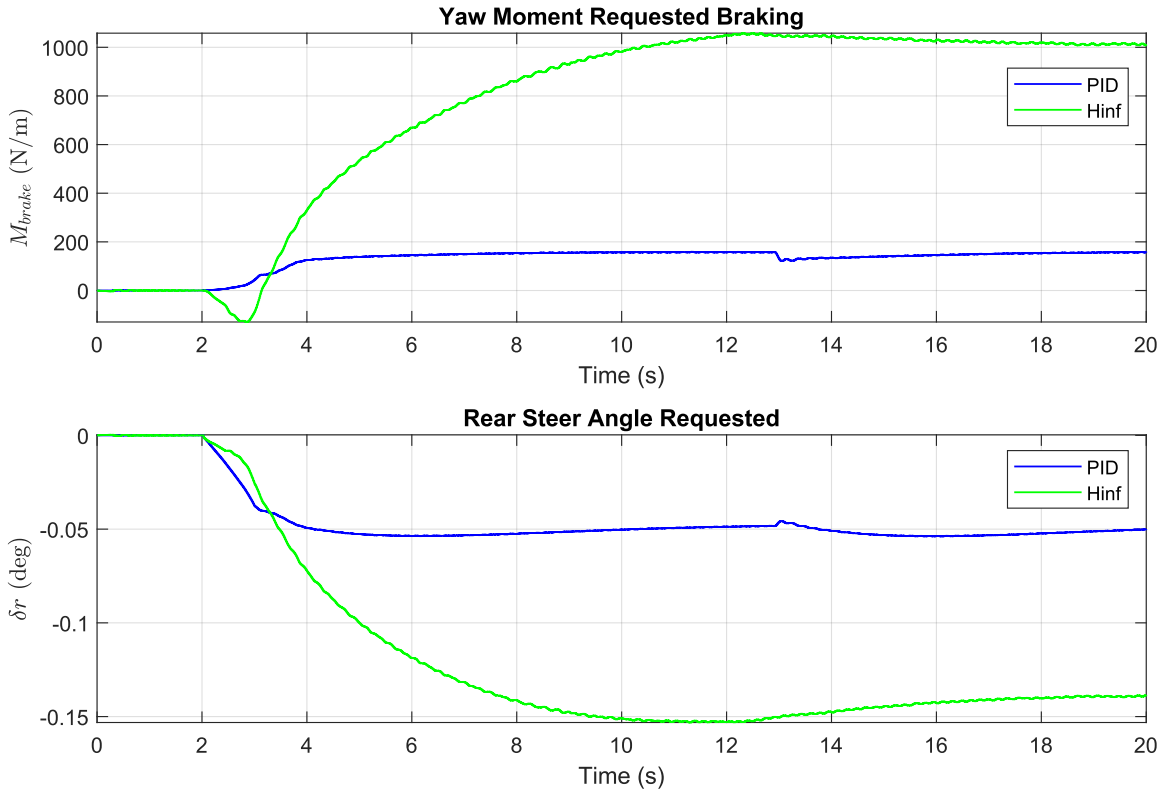

Source: The Author.

The Figure 35 illustrates that the output of the VMC using with $\mathcal{H}_\infty$ controller is 400% stronger than the the PID, for an improvement of 20% in the reference tracking.

	PID	$\mathcal{H}_\infty$
M_{brake}	161.868	505.169
δ_r	-0.051	-0.081

Table 4 – Comparison of total variance of the VMC output PID and $\mathcal{H}_\infty$

Evaluating the variance of the subsequent samples of M_{brake} and δ_r presented in Table 4, it shows that the PID varies less and has a smaller magnitude than the $\mathcal{H}_\infty$.

Taking into account the findings and results outlined in the preceding sections, discussions with the supervisor led to the conclusion that the PID controller offers superior stability, is easier to tune by someone without knowledge in automation and strikes a better balance between robustness and strength of the control input. Consequently, the company opted to maintain the PID implemented for the yaw rate controller. After the tests in the real vehicle, it was found that the PID controller presented low gains, so it was retuned based on the frequency response of the $\mathcal{H}_\infty$ control.

However, this project played an important role in determining that the current PID configuration represents a relativity robust solution within the framework of the VMC

project. Furthermore, this comparison served as a milestone in the project's progress. Moreover, it led to the creation of a patent for the second $\mathcal{H}_\infty$ controller scheme.

Given the $\mathcal{H}_\infty$ controller's ability to achieve satisfactory results in tests with only tuning through virtual environments like MATLAB, the company has proposed researching a new strategy that combines the advantages of both controllers: the simplicity of PID with smoother control inputs and the robustness of $\mathcal{H}_\infty$. Consequently, a study was conducted on Gain Scheduling PID controller incorporating $\mathcal{H}_\infty$ methods, as detailed in the next Chapter.

4 A GAIN-SCHEDULED PID APPROACH FOR LATERAL DYNAMICS

In this chapter, an evolution of the current PID controller will be presented. As discussed, the company made the decision to continue with the PID controller instead of the $\mathcal{H}_\infty$ controller, which exhibited promising results but proved to have a sub-optimal trade-off between control input power and reference tracking when compared to the available controller. The subsequent Section of the dissertation is dedicated to improving the existing PID controller. To achieve this, the focus shifted towards studying a gain-scheduling technique using the $\mathcal{H}_\infty$ method. The goal is to eliminate the need for a lookup table and mitigate the associated challenges that arise from its usage. Since the project is ongoing, this dissertation will present only the study phase.

4.1 FUNDAMENTALS OF GAIN SCHEDULING PID CONTROLLER

A GS Controller is developed using a Linear Parameter-Varying (LPV) systems, which are time linear varying plants whose state space matrices are fixed functions of one or more varying parameters ρ defined as:

$$\begin{cases} \dot{x}(t) = A(\rho(t))\ x(t) + B(\rho(t))\ u(t) \\ y(t) = C(\rho(t))\ x(t) + D(\rho(t))\ u(t), \end{cases} \tag{41}$$

where $x(t) \in R^n$ is the states, $u(t) \in R^m$ control input and $y(t) \in R^l$ measured output. The matrix function $A(\rho(t)) \in R^{nxn}$ and $B(\rho(t)) \in R^{nxm}$ are assumed to depend on the time-varying parameter $\rho(t)$, where $\rho(t) = (\rho_1(t), \rho_2(t), ..., \rho_N(t)) \in U_\rho$. ρ varies in the set of continuously differentiable parameter curves $\rho : [0, \infty) \rightarrow R^N$. It is assumed to be known or measurable and are always assumed to be bounded defined by the minimal $\underline{\rho_i}$ and maximal $\overline{\rho_i}$, $\rho_i(t) \in [\underline{\rho_i}, \overline{\rho_i}], \forall i$.

1. **Stability Conditions**
   To ensure quadratic stability the following parameter dependent Lyapunov function can been chosen:

$$V(x) = x^T\ P(\rho)\ x, \forall x \neq 0 \text{ and } V(0) = 0. \tag{42}$$

   Lemma 1. (GAHINET; APKARIAN; CHILALI, 1996) The LPV system in Equation (41) is quadratic stable, assuming $|\dot{\rho}_i| < \nu_i, \forall i$, if there exists such that

$$A(\rho)^T P(\rho) + P(\rho)A(\rho) + \sum_{i=1}^{N} \nu_i \frac{\partial P(\rho)}{\partial \rho_i} < 0, \forall\ \rho. \tag{43}$$

The use of $\mathcal{H}_\infty$ control principles in gain scheduling adds an additional layer of robustness to the PID approach. By leveraging $\mathcal{H}_\infty$ techniques, the gain-scheduled PID

controller can maintain stability and performance in the presence of uncertainties and disturbances. This strategy combines the simplicity of PID control with the robustness of $\mathcal{H}_\infty$ principles to achieve optimal performance in diverse and dynamic environments.

To define the $\mathcal{H}_\infty$ control problem, four new states have to be included, $x_w(t)$ representing the weighting functions W_i, $e(t)$ the error, $\dot{e}(t)$ the derivative of the error and $u(t)$ the control input. Defined as follows:

$$\begin{cases} z(t) = E(\rho(t))x(t) + F(\rho(t))u(t), \\ \dot{x}_w(t) = A_w(t)x_w(t) + B_{wx}(t)x(t) + B_{wz}(t)z(t), \end{cases} \tag{44}$$

with $z(t)$ being the controlled output.

The output feedback gain-scheduled control law considered for PID controller is in the form:

$$u(t) = K_p(\rho(t))\ e(t) + K_i(\rho(t)) \int_0^t e(t)dt + K_d(\rho(t))\ \dot{e}(t), \tag{45}$$

where $e(t) = y(t) - r(t)$ is the tracking error, $r(t)$ the reference and $K_p(\rho(t))$, $K_i(\rho(t))$, $K_d(\rho(t))$ are controller gain matrices for MIMO systems and scalar gains for SISO systems. Assuming that $\frac{d\rho}{dt} = 0$ the derivative of $u(t)$ is:

$$\begin{aligned} \dot{u}(t) =& K_p(\rho(t))\ \dot{e}(t) + K_i(\rho(t))\ e(t)dt + K_d(\rho(t))\ \ddot{e}(t), \\ =& \begin{bmatrix} Kp(\rho(t))\ Ki(\rho(t))\ Kd(\rho(t)) \end{bmatrix} \begin{bmatrix} \dot{e}(t) \\ e(t) \\ \ddot{e}(t) \end{bmatrix}. \end{aligned} \tag{46}$$

Considering that the $\ddot{r}(t) = 0$, the second derivative of the error can be written as:

$$\begin{aligned} \ddot{e}(t) =& \ddot{r}(t) - \ddot{y}(t), \\ =& -\frac{d^2}{dt^2}\left(C(\rho(t))\ x(t) + D(\rho(t))\ u(t)\right), \\ =& M(\rho(t))\ x(t) + H(\rho(t))\ u(t)). \end{aligned} \tag{47}$$

The augmented model, can be defined as:

$$\left[\begin{array}{c} \dot{x} \\ \dot{x}_w \\ \hdashline \dot{e} \\ \ddot{e} \\ \hdashline \dot{u} \end{array}\right] = \left[\begin{array}{c:c:c:c:c} A(\rho(t)) & 0 & 0 & 0 & B(\rho(t)) \\ \hdashline B_{wx} + B_{wz}C(\rho(t)) & A_w & 0 & 0 & B_{wz}D(\rho(t)) \\ \hdashline 0 & 0 & 0 & I & 0 \\ \hdashline M(\rho(t)) & 0 & 0 & 0 & H(\rho(t)) \\ \hdashline K_d(\rho(t))M(\rho(t)) & 0 & K_i(\rho(t)) & K_p(\rho(t)) & K_d(\rho(t))H(\rho(t)) \end{array}\right] \left[\begin{array}{c} x \\ x_w \\ \hdashline e \\ \dot{e} \\ \hdashline u \end{array}\right]$$

The $\mathcal{H}_\infty$ control problem can be defined as: Find a LPV controller $K(\rho)$ for a system P s.t the close loop system $CL(\rho(t))$ is stable and

$$\|T_z w\|_\infty < \gamma_\infty, \text{ with } \gamma_\infty > 0. \tag{48}$$

The minimum norm γ_∞^* computed as follows:

$$\gamma_\infty^* = \min_{(A_K, B_K, C_K, D_K)} \| T_z w \|_\infty. \tag{49}$$

The solution is base on the use of the Bounded Real Lemma that leads to an LMI problem to be solved over a sufficiently dense grid of points in the scheduling space $\rho \in P$:

$$\begin{bmatrix} A_{CL}^T(\rho)P(\rho) + P(\rho)A_{CL}(\rho) + \sum_{i=1}^{N} \nu_i \frac{\partial P(\rho)}{\partial \rho_i} + & P(\rho)B_{CL}(\rho) & C_{CL}^T(\rho) \\ B_{CL}^T(\rho)P(\rho) & -\gamma_\infty I & D_{CL}^T(\rho) \\ C_{CL}(\rho) & D_{CL}(\rho) & -\gamma_\infty I \end{bmatrix} < 0. \tag{50}$$

Solving the LMIs presented, it can be concluded that the final control will be in the form of:

$$\begin{cases} K_p(\rho(t)) = K_{p0} + K_{p1}\rho_1 + ... + K_{pN}\rho_N \\ K_i(\rho(t)) = K_{i0} + K_{i1}\rho_1 + ... + K_{iN}\rho_N \\ K_d(\rho(t)) = K_{d0} + K_{d1}\rho_1 + ... + K_{dN}\rho_N \end{cases} \tag{51}$$

The practical application of this study for the use case of yaw rate control will not be presented in this dissertation, as it is still under development.

5 CONCLUSION

The final chapter of this document concludes the presented work and outlines the next tasks within the VMC project. The first section provides a conclusive summary of the dissertation, highlighting the accomplishment of the proposed objectives. Then, in the second section, the future works are described, as they provide continuity to the development.

5.1 CONCLUSIVE SUMMARY

This document presents the development of a robust direct yaw moment $\mathcal{H}_\infty$ control system aimed at improving vehicle handling stability to replace the current controller employed by the company. A literature survey provided valuable insights into the theory behind yaw motion control, vehicle modeling and application of $\mathcal{H}_\infty$ control to lateral dynamics.

Based on the gathered information and the requirements of the use case, two $\mathcal{H}_\infty$ controllers were developed using a (linear) bicycle model and consistent weights for realistic performance objectives. Further simulations were conducted with the other subsystems in the VMC project using a complex vehicle model and tests were performed on the actual vehicle to evaluate performance, stability and robustness.

The simulation results showed that both $\mathcal{H}_\infty$ controllers were stable for tire/road contact friction coefficients between $[1, 0.7]$, representing high and mid μ configurations, and were robust across high, medium and low mass scenarios. However, some downsides were observed, such as the controller's strength, which generated a relatively high rear steering angle and yaw braking moment within the VMC project. This issue is believed to be solvable with a more complex controller. The second $\mathcal{H}_\infty$ controller scheme showed better tracking error and lower control input but exhibited more oscillation in the yaw moment, which, although initially concerning, was not observed during vehicle tests.

During tests at the Renault testing center, the 'simpler' $\mathcal{H}_\infty$ controller proved too strong and was not tested on the tracks. However, the second controller scheme demonstrated stability and satisfactory robustness across different driving modes and operating points, though it was still considered to be strong and is currently patented by the company.

Comparing both $\mathcal{H}_\infty$ controllers with the current PID controller, it was concluded that the PID controller offers superior stability, is easier to tune and strikes a better balance between robustness and control input strength. Consequently, the company decided to maintain the PID controller for yaw rate control.

Given the $\mathcal{H}_\infty$ controller's satisfactory performance in virtual environment tuning, a study was conducted on a Gain Scheduling PID controller incorporating $\mathcal{H}_\infty$ methods,

as an option to eliminate the lookup table in the current PID controller.

In conclusion, the main objective of this dissertation project was achieved. A robust $\mathcal{H}_\infty$ controller was developed, presenting room for further improvement, yet delivering satisfying results in simulations and vehicle tests. This work marked a significant milestone in the VMC project and provided a valuable foundation for future developments.

5.2 FUTURE WORK

Based on the conclusions drawn in this dissertation, the $\mathcal{H}_\infty$ controller has demonstrated robustness and effective tuning for real vehicle tests, even when tuned only through simulation. This underscores the $\mathcal{H}_\infty$ method's capability to deliver strong results and reduce the need for extensive tuning tests. Moving forward, this section discusses potential options for enhancing control performance.

One promising direction is the implementation of gain scheduling PID control, as detailed in Chapter 4. This approach has demonstrated promising results in the literature (PEIXOTO; COUTINHO; PALHARES, 2021) and can help the company avoid extensive track testing.

Additionally, the development of a μ synthesis controller (PRASAD; PARIMI, 2022) represents another avenue for potential improvement. Unlike $\mathcal{H}_\infty$, μ synthesis directly incorporates uncertainties, potentially enhancing both robustness and effectiveness.

REFERENCES

ARIPIN, M. K.; MD SAM, Yahaya; DANAPALASINGAM, Kumeresan A.; PENG, Kemao; HAMZAH, N.; ISMAIL, M. F. A Review of Active Yaw Control System for Vehicle Handling and Stability Enhancement. **International Journal of Vehicular Technology**, v. 2014, p. 1–15, 12 June 2014. ISSN 1687-5702, 1687-5710. DOI: 10.1155/2014/437515. Available from: https://www.hindawi.com/journals/ijvt/2014/437515/. Visited on: 19 May 2024.

ARIPIN, MK; MD SAM, Yahaya; DANAPALASINGAM, Kumeresan A; PENG, Kemao; HAMZAH, N; ISMAIL, MF. A review of active yaw control system for vehicle handling and stability enhancement. **International journal of vehicular technology**, Hindawi, v. 2014, 2014.

CANALE, Massimo; FAGIANO, Lorenzo. Comparing rear wheel steering and rear active differential approaches to vehicle yaw control. **Vehicle System Dynamics**, Taylor & Francis, v. 48, n. 5, p. 529–546, 2010.

CHEN, Chieh; TOMIZUKA, Masayoshi. Lateral control of commercial heavy vehicles. **Vehicle System Dynamics**, Taylor & Francis, v. 33, n. 6, p. 391–420, 2000.

D'ANDREA, Raffaello. LMI Approach to Mixed H-2 and H-infinity Performance Objective Controller Design. **IFAC Proceedings Volumes**, v. 29, n. 1, p. 3198–3203, 1996. ISSN 1474-6670. DOI: https://doi.org/10.1016/S1474-6670(17)58168-9. Available from: https://www.sciencedirect.com/science/article/pii/S1474667017581689.

DING, Nenggen; TAHERI, Saied. An adaptive integrated algorithm for active front steering and direct yaw moment control based on direct Lyapunov method. **Vehicle System Dynamics**, Taylor & Francis, v. 48, n. 10, p. 1193–1213, 2010.

DOUMIATI, M.; SENAME, O.; MARTINEZ, J.; DUGARD, L.; POUSSOT-VASSAL, C. Gain-scheduled LPV/H controller based on direct yaw moment and active steering for vehicle handling improvements. In: 49TH IEEE Conference on Decision and Control (CDC). [S.l.: s.n.], 2010. P. 6427–6432. DOI: 10.1109/CDC.2010.6171089.

DOUMIATI, Moustapha; SENAME, Olivier; MARTINEZ MOLINA, John Jairo; DUGARD, Luc; GASPAR, Peter; SZABO, Zoltan; BOKOR, Jozsef. LPV/Hinf controller for vehicle handling and stability enhancement. In: VSDIA 2010 - 12TH MINI

CONFERENCE ON VEHICLE SYSTEM DYNAMICS, IDENTIFICATION AND ANOMALIES. Budapest, Hungary: [s.n.], Nov. 2010. P. 12. Available from: https://hal.science/hal-00536313.

DU, Haiping; ZHANG, Nong; NAGHDY, Fazel. Velocity-dependent robust control for improving vehicle lateral dynamics. **Transportation research part C: emerging technologies**, Elsevier, v. 19, n. 3, p. 454–468, 2011.

GAHINET, P.; APKARIAN, P.; CHILALI, M. Affine parameter-dependent Lyapunov functions and real parametric uncertainty. **IEEE Transactions on Automatic Control**, v. 41, n. 3, p. 436–442, 1996. DOI: 10.1109/9.486646.

GAO, Feng; LI, Shengbo Eben; ZHENG, Yang; KUM, Dongsuk. Robust control of heterogeneous vehicular platoon with uncertain dynamics and communication delay. **IET Intelligent Transport Systems**, v. 10, n. 7, p. 503–513, 2016. DOI: https://doi.org/10.1049/iet-its.2015.0205. eprint: https://ietresearch.onlinelibrary.wiley.com/doi/pdf/10.1049/iet-its.2015.0205. Available from: https://ietresearch.onlinelibrary.wiley.com/doi/abs/10.1049/iet-its.2015.0205.

JIN, Xian Jian; YIN, Guodong; CHEN, Nan. Gain-scheduled robust control for lateral stability of four-wheel-independent-drive electric vehicles via linear parameter-varying technique. **Mechatronics**, v. 30, p. 286–296, 2015. ISSN 0957-4158. DOI: https://doi.org/10.1016/j.mechatronics.2014.12.008. Available from: https://www.sciencedirect.com/science/article/pii/S0957415814002153.

KISSAI, Moad. **Optimal Coordination of Chassis Systems for Vehicle Motion Control**. June 2019. Theses – Université Paris Saclay (COmUE). Available from: https://pastel.hal.science/tel-02292877.

LACROIX, Benoit; LIU, Zhao Heng; SEERS, Patrice. A Comparison of Two Control Methods for Vehicle Stability Control by Direct Yaw Moment. In: PRODUCT Design and Manufacture. [S.l.]: Trans Tech Publications Ltd, Jan. 2012. (Applied Mechanics and Materials), p. 203–217. DOI: 10.4028/www.scientific.net/AMM.120.203.

LOFBERG, J. YALMIP : a toolbox for modeling and optimization in MATLAB. In: 2004 IEEE International Conference on Robotics and Automation (IEEE Cat. No.04CH37508). [S.l.: s.n.], 2004. P. 284–289. DOI: 10.1109/CACSD.2004.1393890.

MINOIU ENACHE, Nicoleta. **Assistance préventive à la sortie de voie**. Nov. 2008. Theses – Université d'Evry-Val d'Essonne. Available from: https://theses.hal.science/tel-00364073.

NAEEM, Hafiz Muhammad Yasir; MAHMOOD, A. Robust and optimal control of longitudinal dynamics of automotive vehicle. In: 2017 International Conference on Electrical Engineering (ICEE). [S.l.: s.n.], 2017. P. 1–6. DOI: 10.1109/ICEE.2017.7893426.

PACEJKA, Hans B. **Tyre and Vehicle Dynamics**. Second Edition. [S.l.]: Elsevier, 2006. ISBN 978-0-7506-6918-4. DOI: 10.1016/B978-0-7506-6918-4.X5000-X. Available from: https://linkinghub.elsevier.com/retrieve/pii/B9780750669184X5000X. Visited on: 19 June 2024.

PEIXOTO, Márcia L. C.; COUTINHO, Pedro Henrique Silva; PALHARES, Reinaldo Martínez. Improved robust gain-scheduling static output-feedback control for discrete-time LPV systems. **Eur. J. Control**, v. 58, p. 11–16, 2021. Available from: https://api.semanticscholar.org/CorpusID:232041423.

PRASAD, P. Shambhu; PARIMI, Alivelu Manga. Robust μ-Synthesis Controller Design and Analysis for Load Frequency Control in an AC Microgrid System. **IFAC-PapersOnLine**, 2022. Available from: https://api.semanticscholar.org/CorpusID:248682280.

RAJAMANI, Rajesh. **Vehicle Dynamics and Control**. Boston, MA: Springer US, 2012. (Mechanical Engineering Series). ISBN 978-1-4614-1432-2 978-1-4614-1433-9. DOI: 10.1007/978-1-4614-1433-9. Available from: https://link.springer.com/10.1007/978-1-4614-1433-9. Visited on: 20 May 2024.

VESELÝ, Vojtech; ILKA, Adrian. Gain-scheduled PID controller design. **Journal of Process Control**, v. 23, n. 8, p. 1141–1148, 2013. ISSN 0959-1524. DOI: https://doi.org/10.1016/j.jprocont.2013.07.002. Available from: https://www.sciencedirect.com/science/article/pii/S0959152413001388.

WU, Jianyong; WANG, Qingping; WEI, Xue; TANG, Houjun. Studies on improving vehicle handling and lane keeping performance of closed-loop driver–vehicle system with integrated chassis control. **Mathematics and Computers in Simulation**, Elsevier, v. 80, n. 12, p. 2297–2308, 2010.

YIN, Guodong; CHEN, Nan; LI, Pu. Improving Handling Stability Performance of Four-Wheel Steering Vehicle via μ-Synthesis Robust Control. **IEEE Transactions on Vehicular Technology**, v. 56, n. 5, p. 2432–2439, 2007. DOI: 10.1109/TVT.2007.899941.

ZHAO, Chenming; XIANG, Weidong; RICHARDSON, Paul. Vehicle lateral control and yaw stability control through differential braking. In: IEEE. 2006 IEEE international symposium on industrial electronics. [S.l.: s.n.], 2006. P. 384–389.

ZHOU, Hao; CHEN, Hong; REN, Bingtao; ZHAO, Haiyan. Yaw stability control for in-wheel-motored electric vehicle with a fuzzy PID method. In: THE 27th Chinese Control and Decision Conference (2015 CCDC). [S.l.: s.n.], 2015. P. 1876–1881. DOI: 10.1109/CCDC.2015.7162225.

ZHOU, Hongliang; LIU, Zhiyuan. Vehicle Yaw Stability-Control System Design Based on Sliding Mode and Backstepping Control Approach. **IEEE Transactions on Vehicular Technology**, v. 59, n. 7, p. 3674–3678, 2010. DOI: 10.1109/TVT.2010.2050790.

ZHOU, Kemin; KHARGONEKAR, Pramod P. An algebraic Riccati equation approach to H optimization. **Systems & Control Letters**, v. 11, n. 2, p. 85–91, 1988. ISSN 0167-6911. DOI: https://doi.org/10.1016/0167-6911(88)90080-1. Available from: https://www.sciencedirect.com/science/article/pii/0167691188900801.